Journal for ImmunoTherapy of Cancer

Combining IL-2-based immunotherapy with commensal probiotics produces enhanced antitumor immune response and tumor clearance

Linlin Shi,[1] Jianyong Sheng ,[1] Guozhong Chen,[2] Peng Zhu,[3] Changping Shi,[2] Bei Li,[2] Chaiwoo Park,[2] Jingyi Wang,[4] Bixiang Zhang,[3] Zhi Liu ,[2] Xiangliang Yang[1]

To cite: Shi L, Sheng J, Chen G, *et al*. Combining IL-2-based immunotherapy with commensal probiotics produces enhanced antitumor immune response and tumor clearance. *Journal for ImmunoTherapy of Cancer* 2020;**8**:e000973. doi:10.1136/jitc-2020-000973

► Additional material is published online only. To view please visit the journal online (http://dx.doi.org/10.1136/jitc-2020-000973).

LS and JS contributed equally.

Accepted 20 August 2020

For numbered affiliations see end of article.

Correspondence to
Professor Zhi Liu;
zhiliu@hust.edu.cn

Professor Bixiang Zhang;
bixiangzhang@163.com

Professor Xiangliang Yang;
yangxl@hust.edu.cn

ABSTRACT

Background Interleukin-2 (IL-2) serves as a pioneer of immunotherapeutic agent in cancer treatment. However, there is a considerable proportion of patients who cannot benefit from this therapy due to the limited clinical responses and dose-limiting toxicities. Mounting evidence indicates that commensal microbiota shapes the outcome of cancer immunotherapies. In this study, we aim to investigate the enhancing effect of *Akkermansia muciniphila* (AKK), a beneficial commensal microbe receiving considerable attentions, on the antitumor efficacy of IL-2 and explore the underlying molecular mechanism.

Methods Colorectal carcinoma patient-derived tumor tissues were used to evaluate the therapeutic efficacy of combination treatment. AKK was orally delivered to B16F10 and CT26 tumor-bearing mice along with systemic IL-2 treatment. Flow cytometry was carried out to analyze the tumor immune microenvironment. The molecular mechanism of the enhanced therapeutic efficacy was explored by RNA-seq and then verified in tumor-bearing mice.

Results Combined treatment with IL-2 and AKK showed a stronger antitumor efficacy in colorectal cancer patient-derived tumor tissues. Meanwhile, the therapeutic outcome of IL-2 was significantly potentiated by oral administration of AKK in subcutaneous melanoma and colorectal tumor-bearing mice, resulting from the strengthened antitumor immune surveillance. Mechanistically, the antitumor immune response elicited by AKK was partially mediated by Amuc, derived from the outer membrane protein of AKK, through activating toll-like receptor 2 (TLR2) signaling pathway. Besides, oral supplementation with AKK protected gut barrier function and maintained mucosal homeostasis under systemic IL-2 treatment.

Conclusion These findings propose that IL-2 combined with AKK is a novel therapeutic strategy with prospecting application for cancer treatment in clinical practice.

BACKGROUND

Long-term remissions have been shown among some patients with cancer in the recent clinical trials of cancer immunotherapy, mainly including the redirected chimeric antigen receptor T cells, antibodies targeting cytotoxic T lymphocyte antigen-4 (CTLA-4) or programmed death-1 (PD-1).[1 2] Cancer immunotherapies are designed to fire up the patients' own immune system to fight against cancer and have picked up considerable momentum in clinical practices.[3] However, each strategy still faces many challenges in eliminating hematological neoplasms and especially solid tumors, resulting from the primary or acquired resistance, unpredictable hyperprogression and immune-related toxicities.[4–6]

Interleukin 2 (IL-2) is a protein that stimulates T-cell proliferation, augments cytotoxic activity of natural killer cells and triggers proinflammatory cytokine release.[7] Notably, IL-2 is the first cancer immunotherapeutic drug approved by the US Food and Drug Administration (FDA) decades ago for the treatment of metastatic melanoma and renal cell carcinoma.[8] However, due to the complexity of IL-2-induced toxicities including vascular leak syndrome, pulmonary edema, nausea and diarrhea, patients receiving high dose of IL-2 must be closely monitored.[9] Therefore, physicians are usually deliberative to choose IL-2 treatment, which limits its clinical application as a monotherapy.[10] Alternatively, IL-2 in relatively low dose is safer but hinders its antitumor efficacy.[9 10] In detail, IL-2 has limited effect in reversing immunosuppressive tumor microenvironment and in some cases even proliferates regulatory T cells (Tregs), which is regarded as the crucial limiting factor in tumor eradication and is closely associated with poor clinical response.[8–10] Therefore, combination treatments with other therapeutic approaches are needed to restore the efficacy of IL-2-based immunotherapy.

There is growing evidence that the interindividual variability in gut microbiota accounts for the significant heterogeneity in therapeutic responses to cancer immunotherapy.[11 12] Both preclinical studies and clinical trials have highlighted the important roles of gut microbiota in immune checkpoint inhibitor therapies.[13 14] Oral administration with antibiotics resulted in shorter progression-free survival and overall survival in patients receiving PD-1 blockade immunotherapy, indicating that gut dysbiosis significantly compromised the clinical benefit of immune checkpoint blockade immunotherapies.[13] Gut microbiota serves as biomarkers in predicting potential clinical response, and thus, targeting it may have important guidance to those non-responders under immunotherapies.[15 16]

Akkermansia muciniphila (AKK), an intestinal symbiont colonizing on the mucosal layer, plays important roles in ameliorating host metabolic disorders[17] and improving immune responses.[18–20] Moreover, the correlation between AKK and cancer immunotherapy receives increasing attentions.[13 19] AKK is significantly enriched in immune checkpoint blockade responding patients, revealing that it is associated with a stronger antitumor immune response and favorable clinical outcome.[13] Besides, tumor size was significantly shrunk in the mice receiving fecal microbiota transplantation from immune checkpoint blockade responders with a higher abundance of AKK in the gut microbiota.[13] However, the specific cellular and molecular links between AKK-elicited antitumor efficiency and host immune response in the context of cancer immunotherapy remain unclear.[21] We hypothesize that combination treatment with IL-2 and AKK may serve as a potential approach to restore the therapeutic efficacy of IL-2-based immunotherapy and reduce its gastrointestinal side effects, thus making this old drug get fresh look in cancer treatment.

In the current study, therapeutic efficacy of combined treatment with IL-2 and AKK was evaluated in colorectal cancer (CRC) patient-derived tumor tissues and B16F10 or CT26 tumor-bearing mice. Accordingly, alterations of tumor microenvironment among different groups were investigated and the underlying mechanism of the antitumor immune response induced by AKK was further explored. Furthermore, the protective effects of AKK treatment on gut barrier and commensal microbiota homeostasis were studied in the context of IL-2-based immunotherapy. Collectively, these findings provide the first basis that combination treatment of IL-2 and AKK is an effective and safe therapeutic strategy with potential clinical applications, thus shedding new lights on cancer immunotherapy (figure 1).

METHODS

Bacteria and cell lines

AKK (ATTC BAA-835) was cultured in a basal medium containing 0.25% w/v mucin at 37°C, pH 6.5 under strict anaerobic conditions. Murine melanoma cell line B16F10 (syngeneic with C57BL/6 mice) was cultured with Dulbecco's Modified Eagle Medium (DMEM) containing 100 µg/mL of streptomycin and 100 IU/mL of penicillin and supplemented with 10% fetal bovine serum. Murine colon carcinoma cell line CT26 (syngeneic with Balb/c mice) was cultured with Roswell Park Memorial Institute (RPMI) 1640 Medium containing 100 µg/mL of streptomycin and 100 IU/mL of penicillin and supplemented with 10% fetal bovine serum. Both cells were grown in a humidified incubator at 37°C with 5% CO_2.

Isolation and treatment of CRC patient-derived tumor tissues

Primary CRC specimens were obtained from patients who received surgical resection at Tongji Hospital of Huazhong University of Science and Technology. Fresh tumor tissues were washed twice with DMEM (Gibco) containing 5% fetal bovine serum (FBS), 100 U/mL penicillin and 100 µg/mL streptomycin, cut into small pieces of 2–4 mm and followed by removal of fat and necrotic areas. Then, they were digested at 37°C for 30 min by using the tumor dissociation kit (Miltenyi Biotec, California, USA), filtered into single cell suspensions through a 70 µm nylon cell strainer (BD Falcon, USA) and followed by regular cell culture (DMEM plus 10% FBS). Cells were then subjected to different treatments. After the single treatment of IL-2 (10 ng/mL) and AKK (1×10^7 CFU/mL) or the combination treatment for 24 hours, tumor cell apoptosis and tumor immune microenvironment were analyzed by flow cytometry.

Tumor-bearing mouse models

Female 6-week-old to 8-week-old Balb/c mice were purchased from Hubei Province Center for Disease Control and Prevention (Wuhan, China). Female 6-week-old to 8-week-old C57BL/6 mice were purchased from Beijing Vital River Laboratory Animal Technology Co (Beijing, China). All mice were housed in a specific pathogen-free environment at a constant temperature (22°C±3°C), with a 12-hour light/dark cycle and fed adaptively for 1 week after arrival. During the experiments, all mice received the humane care and had free access to water and the maintenance diet.

In melanoma model, mice were inoculated subcutaneously with injections of 2×10^5 B16F10 tumor cells into their right flanks. In murine CRC model, mice were challenged subcutaneously with 5×10^5 CT26 tumor cells instead. Mice in each model were randomly divided into four groups (n=6). For the AKK group, each mouse was treated with an oral administration of 1×10^8 colony-forming units (CFU) (suspended in 200 µL of saline) every 3 days on the day of tumor inoculation and the treatment lasted for 23 days in melanoma model and 25 days in CRC model, respectively. For the IL-2 group, mice were intravenously injected with IL-2 at a dose of 2.5 µg/kg every 3 days for four times. For the combination therapy group, mice were treated with IL-2 along with AKK as described above, respectively. For the control group, 200 µL of saline was administrated to mice by oral gavage or intravenous injection. Tumor

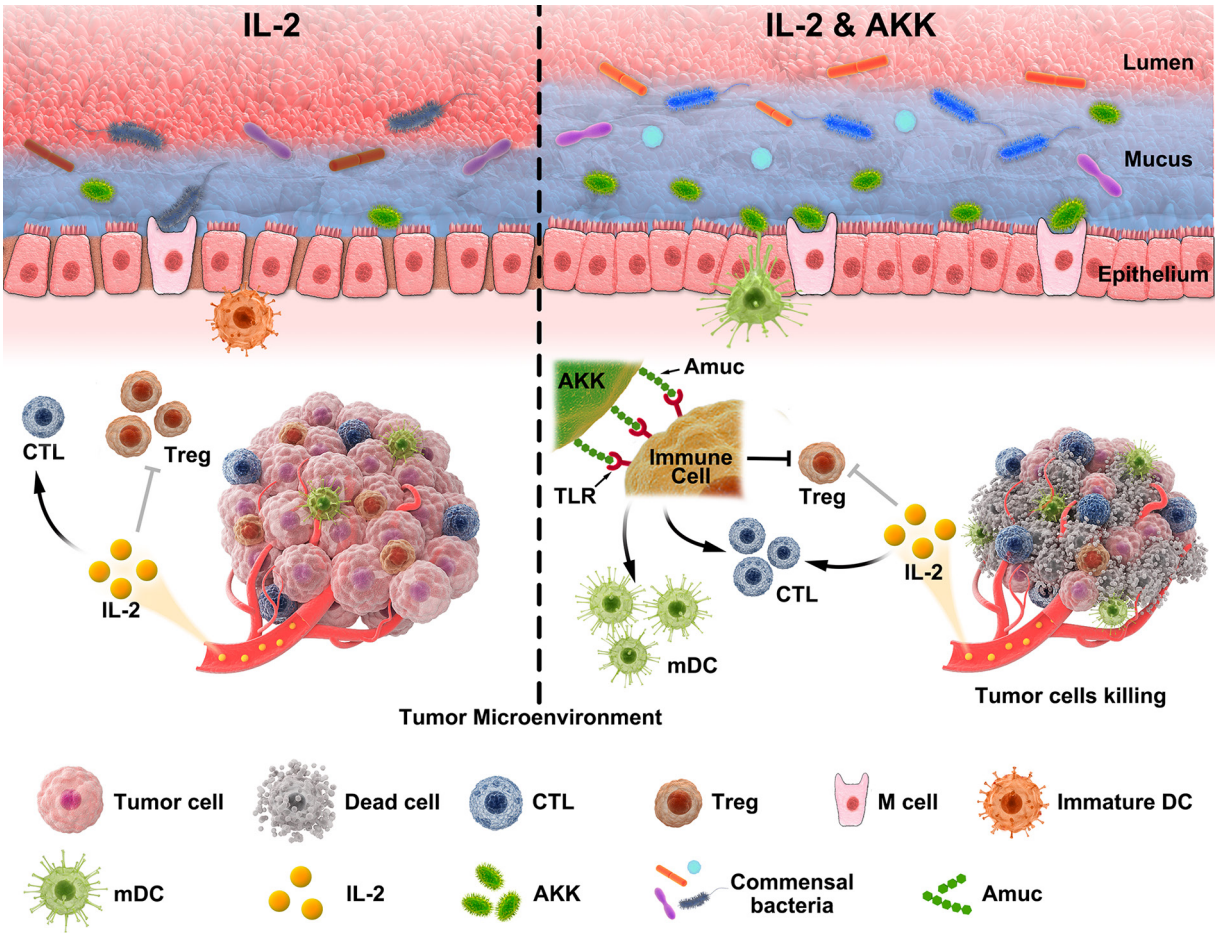

Figure 1 Schematic illustration of the combined treatment of IL-2 and AKK in tumor suppression. AKK restores the therapeutic efficacy of IL-2 to trigger a stronger antitumor immune response, which is initiated from the activation of TLR2 signaling pathway via its outer membrane protein Amuc. Moreover, AKK improves the integrity of intestinal barrier and gut microbiota homeostasis in IL-2-treated mice, probably due to the crosstalk between AKK and gut commensal microbiota. AKK, *Akkermansia muciniphila;* CTL, cytotoxic T lymphocyte; DC, dendritic cell; IL-2, interleukin 2; TLR, toll-like receptor.

volume and body weight were recorded every 3 days. The length (L) and width (W) of tumor were measured every 3 days with a digital caliper and tumor volume was calculated as $L \times W^2 \times 0.5$. When the tumor volume reached about 2000 mm^3, mice were sacrificed according to the guidelines for animal care. Tumors were isolated and weighed. In addition, fundus vein blood samples were collected for further study. Fecal samples were collected, snap frozen in sterile microtube immediately and stored at −80°C for subsequent analysis.

Statistical analysis

All values are presented as mean±SD. Statistical analyses were carried out using the GraphPad Prism software V.6.0. Comparison between two groups was performed using unpaired two-tailed Student's t-test. One-way analysis of variance was used for comparison of more than two groups. Values with $p<0.05$ are considered significant.

Additional material and methods

Other detailed materials and methods can be found in online supplemental information.

RESULTS

Therapeutic efficacy of IL-2 combining with AKK in CRC patient-derived ex vivo tumor tissues

Patients with CRC receiving tumor-removal surgery were recruited in this study. The clinical characteristics of the CRC patients are shown in online supplemental table S1. The fresh tumor tissues along with tumor-draining lymph nodes from each patient were collected during the surgery. The isolated tumor tissues were immediately digested and filtered into single cell suspensions and then received different treatments (figure 2A). Combined treatment of IL-2 and AKK resulted in a significant higher rate of apoptosis tumor cells than either IL-2 or AKK treatment alone (figure 2B,F). Meanwhile, to investigate whether the tumor suppressive effect was immune response mediated, tumor-infiltrating lymphocytes were harvested and analyzed by flow cytometry after different treatments. Results showed that AKK treatment alone or in combination with IL-2 increased the ratio of $CD8^+$/$CD4^+$ in $CD3^+$ T cells from tumor-infiltrating lymphocytes, while IL-2 treatment alone did not show obvious difference compared with the phosphate-buffered saline (PBS)

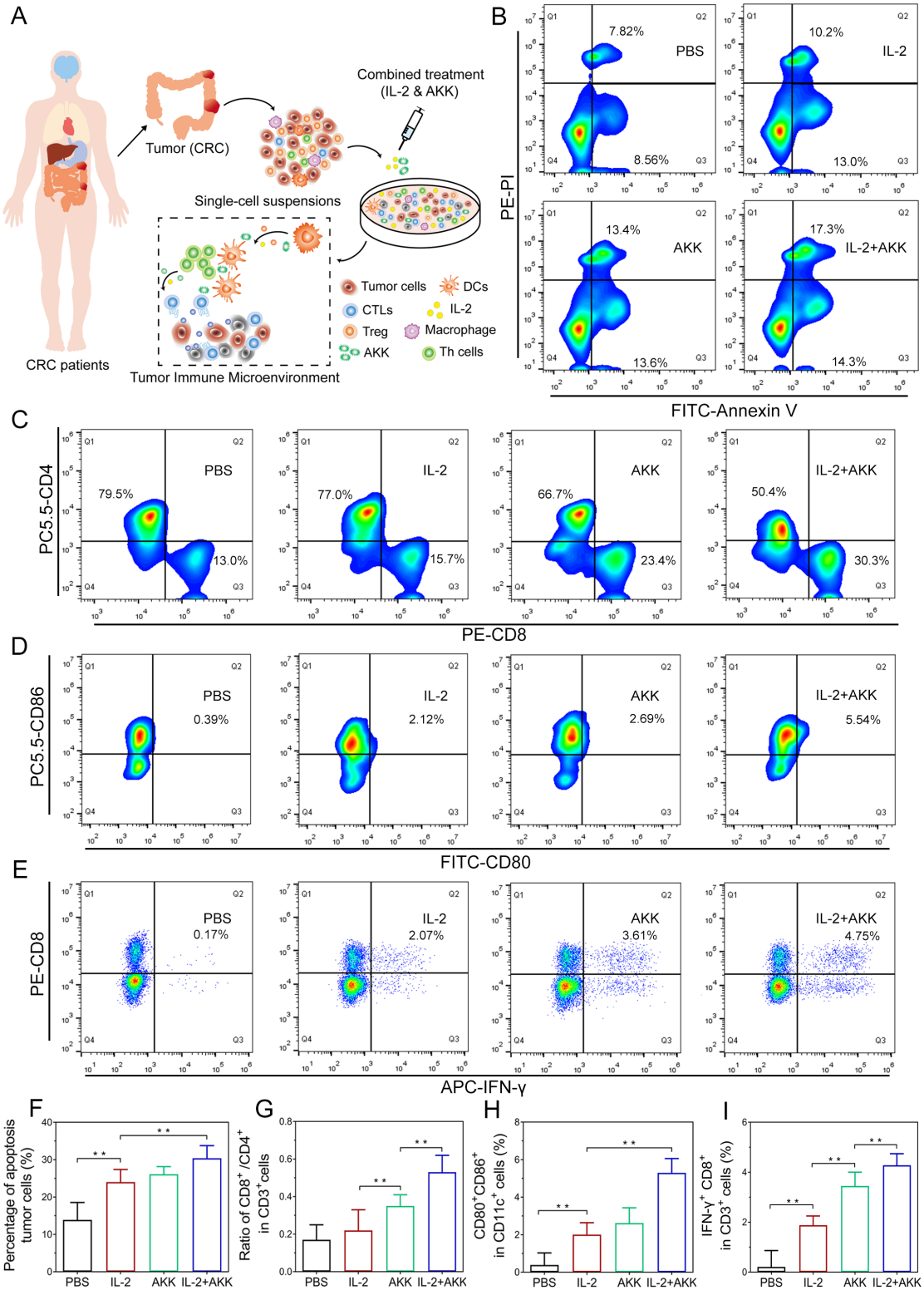

Figure 2 Effects of combination treatment of IL-2 and AKK in ex vivo tumor tissues isolated from patients with CRC. Tumor tissues were dissociated into small pieces, digested and filtrated to generate single-cell suspensions. The cell suspensions were treated with AKK and IL-2 in combination or individually. (A) Schematic illustration of combination treatment of IL-2 and AKK in CRC patient-derived ex vivo tumor tissues. (B) Tumor cells were collected and stained with FITC-conjugated Annexin-V and PI for apoptosis detection by flow cytometry. (C–E) Representative flow cytometry analysis of $CD8^+/CD4^+$ ratio in $CD3^+$ T cells (C), activated DCs (D) and cytotoxic effector T cells (E) in tumor-infiltrating lymphocytes isolated from patients with CRC. (F–I) Percentage of apoptosis tumor cells among different groups (F), ratio of $CD8^+/CD4^+$ in $CD3^+$ T cells (G), $CD80^+$ $CD86^+$ in $CD11c^+$ cells (H) and IFN-γ^+ $CD8^+$ in $CD3^+$ T cells (I). All data are shown as mean±SD (n=3) (**p<0.01). AKK, *Akkermansia muciniphila*; APC, allophycocyanin; CRC, colorectal cancer; CTL, cytotoxic T lymphocyte; DC, dendritic cell; FITC, fluorescein isothiocyanate; IFN, interferon; IL-2, interleukin-2; PBS, phosphate-buffered saline; PE-PI, phycoerythrin-propidium iodide.

treated control (figure 2C,G). Moreover, compared with the single treatment groups, the combination treatment of IL-2 and AKK stimulated the maturation of dendritic cells (DCs) and the activation of cytotoxic T lymphocytes (CTLs) more effectively, as evidenced by a higher proportion of $CD80^+$ $CD86^+$ in $CD11c^+$ cells (figure 2D,H) and IFN-γ^+ $CD8^+$ in $CD3^+$ T cells (figure 2E,I) recruited in tumor-draining lymph nodes. Collectively, these findings suggest that the combination treatment of IL-2 and AKK elicits potent antitumor immune response and promotes tumor cell apoptosis.

Therapeutic response of combination treatment of IL-2 and AKK in tumor-bearing mice

Based on the ex vivo experiments on CRC patient-derived tumor tissues, we wondered whether systemic IL-2 treatment combining with oral administration of AKK can also trigger tumor regression in vivo. The antitumor efficacy of combination therapy was evaluated in CT26 (figure 3A) and B16F10 (figure 3C) tumor-bearing mice models. Single treatment with IL-2 showed moderate therapeutic performance compared with the saline-treated controls, while pretreatment with AKK could significantly slow down the tumor progression. Notably, combined treatment of IL-2 and AKK further prolonged the survival of the tumor-bearing mice compared with IL-2 treatment alone or saline-treated control (figure 3B,D). Consistently, the combined treatment resulted in smaller tumor size and lower weights of the excised tumors (figure 3E,F and online supplemental figure S1). H&E, ki67 and TUNEL staining of the tumor tissue slices showed that the

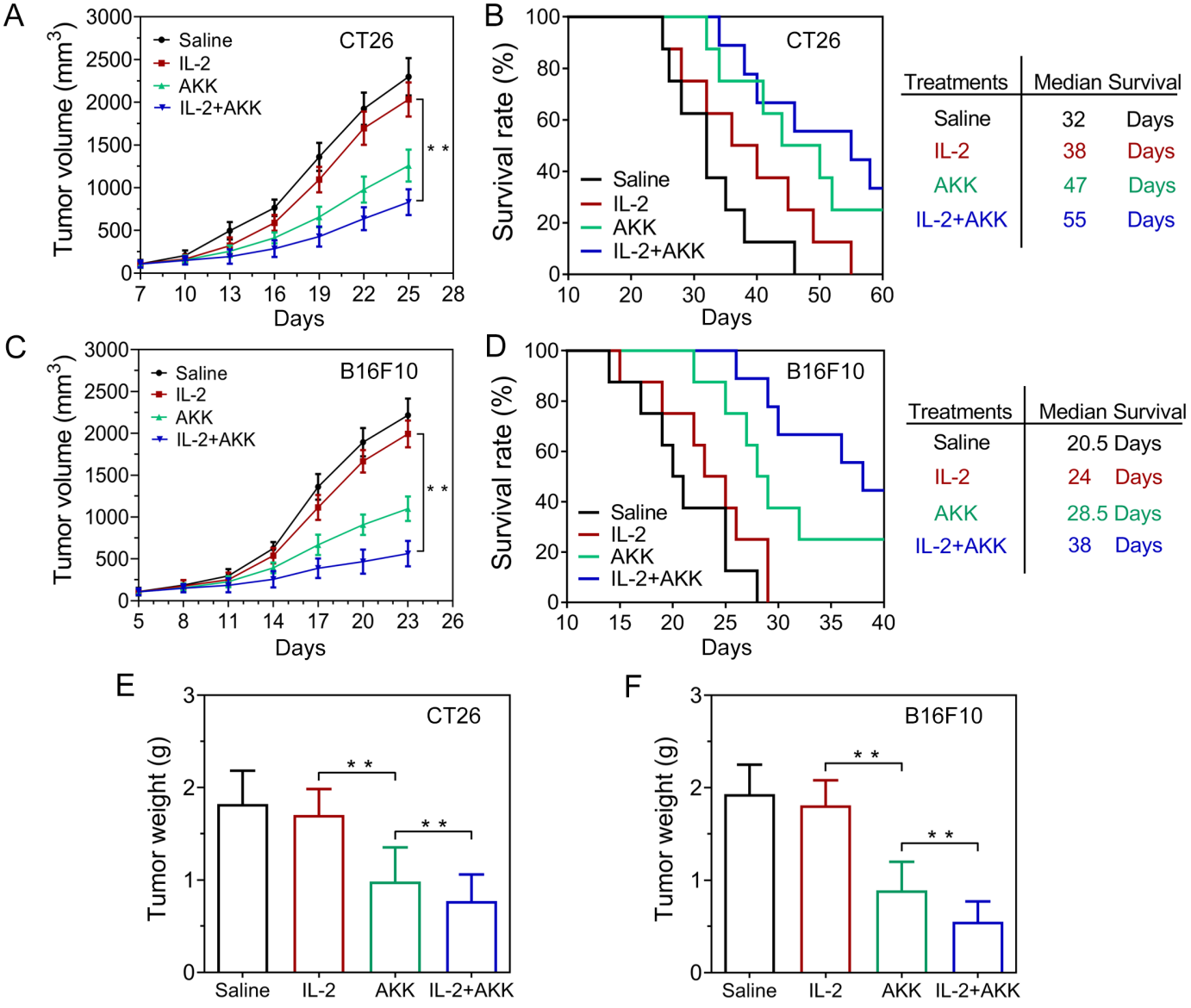

Figure 3 Antitumor efficacy of combination treatment of IL-2 and AKK in CT26 and B16F10 tumor-bearing mice. (A,C) Tumor growth in CT26 (A) and B16F10 (C) tumor-bearing mice (n=6). (B,D) Kaplan-Meier survival rate of CT26 (B) and B16F10 (D) tumor-bearing mice after different treatments (n=8). (E,F) Tumor weight in CT26 tumor-bearing mice (E) and B16F10 tumor-bearing mice (F) at the end of the experiment (n=6). All data are shown as mean±SD (*p<0.05, **p<0.01). AKK, *Akkermansia muciniphila*; IL-2, interleukin-2.

combined therapy induced more necrosis, less cell proliferation and more cell apoptosis compared with the single treatments with IL-2 or AKK (online supplemental figures S2–S5). Together, these results suggest that combination with the treatment of AKK enhances the antitumor efficacy of IL-2 in tumor-bearing mice.

Alterations of tumor immune microenvironment by combination treatment of IL-2 and AKK

Tumor-infiltrating lymphocytes were harvested from different groups of sacrificed tumor-bearing mice and were analyzed by flow cytometry. The combination treatment could effectively recruit a higher proportion of CTLs in tumor-draining lymph nodes compared with the IL-2 treatment alone (figure 4A,C and online supplemental figure S6A). Moreover, administration with AKK alone or in combination with IL-2 significantly decreased the ratio of Tregs in the tumor-draining lymph nodes, while single treatment with IL-2 did not show an obvious inhibitory effect on Tregs (figure 4B,D and online supplemental figure S6B). Importantly, production of proinflammatory cytokines was also induced with the combined treatment, as demonstrated by the significantly elevated levels of IFN-γ and IL-2 in tumor tissues as well as tumor necrosis factor-α (TNF-α) levels in the serum (figure 4E,F,G and online supplemental figure S6C,D). Besides, the immunoinhibitory cytokines of transforming growth factor-β (TGF-β) in the serum were reduced after combined AKK and IL-2 therapy (figure 4H).

The immunosuppressive tumor microenvironment can also be established by tumor-repopulating cells.[22] Targeting these tumorigenic cells will relieve tumor immunosuppression and improve antitumor immune responses.[23] In this study, the proportion of side population cells in the tumor tissues was analyzed by flow cytometry. Combined treatment of IL-2 and AKK significantly reduced the proportion of side population cells compared with single treatment groups, suggesting an attenuated tumor-repopulating cell-like potency (figure 4I and online supplemental figure S8A,C). Besides, single cell suspensions prepared from tumor tissues of CT26 or B16F10 tumor-bearing mice were seeded in soft 3D fibrin gels (stiffness: 90 Pa) and grown for 5 days, respectively. During spheroid formation, tumor cells derived from the combined treatment group resulted in significantly lower colony number and colony size compared with those from the saline-treated controls or the single treatment groups (figure 4J,K and online supplemental figures S7, S8B,D,E). It was also found that combined treatment with IL-2 and AKK significantly reduced the proportion of $CD133^{+}$ cell in tumor tissues compared with the single treatment groups (online supplemental figures S9,S10). These results indicate that the tumor stem cell-like potency is weakened by the combined treatment with IL-2 and AKK in tumor-bearing mice.

Involvement of AKK-derived outer membrane protein in mediating antitumor immune response

We next explored the possible mechanism underlying the immune-mediated antitumor effects of AKK. It was found that pasteurized AKK could still promote tumor regression in subcutaneous CRC and melanoma mouse model (figure 5A and online supplemental figure S11). Besides, the culture supernatants of AKK showed negligible tumor inhibition efficacy, suggesting that the antitumor effects of AKK may not be mediated by AKK-derived metabolites (figure 5B and online supplemental figure S11). Consequently, we expressed and purified one of the most abundant outer membrane protein of AKK, here named Amuc (online supplemental figure S12) which is involved in the crosstalk with the host immune microenvironment.[24] Intriguingly, oral administration of Amuc also significantly improved the therapeutic efficacy of IL-2 against tumor growth (figure 5C and online supplemental figure S13). In parallel, we found that the tumor suppression efficacy of Amuc could be blocked by the Amuc-specific antibody (online supplemental figure S14). To further investigate the contribution of Amuc in the antitumor effects of AKK, AKK was pretreated with the Amuc-specific antibody to block Amuc prior to oral administration to the tumor-bearing mice. Results showed that the antibody treatment largely impaired the tumor suppression efficacy of AKK, suggesting that Amuc played an important role in AKK-induced tumor suppression (figure 5D).

In vitro studies suggest that Amuc has no direct effect on the viability, apoptosis and cell cycle of CT26 or B16F10 tumor cells (online supplemental figures S15, S16). Instead, the antitumor efficacy of Amuc probably derived from stimulation of the systemic antitumor immune response. To testify this assumption, tumor-infiltrating lymphocytes from tumor-bearing mice receiving treatment with Amuc alone or in combination with IL-2 were analyzed by flow cytometry. Results showed that Amuc increased the proportion of CTLs but decreased the proportion of Tregs in tumor immune microenvironment. The combination with IL-2 further enhanced the effects of Amuc in regulating CTLs or Tregs levels (figure 5E–H and online supplemental figure S17). The effect of Amuc in tumor-bearing mice is consistent with the results of AKK in the same tumor-bearing mouse models (figure 4A–D and online supplemental figure S6).

Stimulation of antitumor immune responses by Amuc via TLR2 signaling pathway

To gain better insight into the underlying mechanisms of Amuc-mediated tumor-specific immune response, transcriptomics sequencing was performed on the ex vivo Amuc-treated tumor-infiltrating lymphocytes. Then 3D-principal coordinate analysis (3D-PCoA) was conducted by using the transcriptome data (online supplemental figures S18, S19). The results showed that the gene expression profile of the Amuc-treated group was clearly separated from that of the PBS-treated, indicating that the transcriptome reprogramming occurred in tumor-infiltrating lymphocytes in response to Amuc treatment (figure 6A and online supplemental figure S20). Subsequently, Kyoto Encyclopedia of Genes and Genomes (KEGG) pathway enrichment analysis was

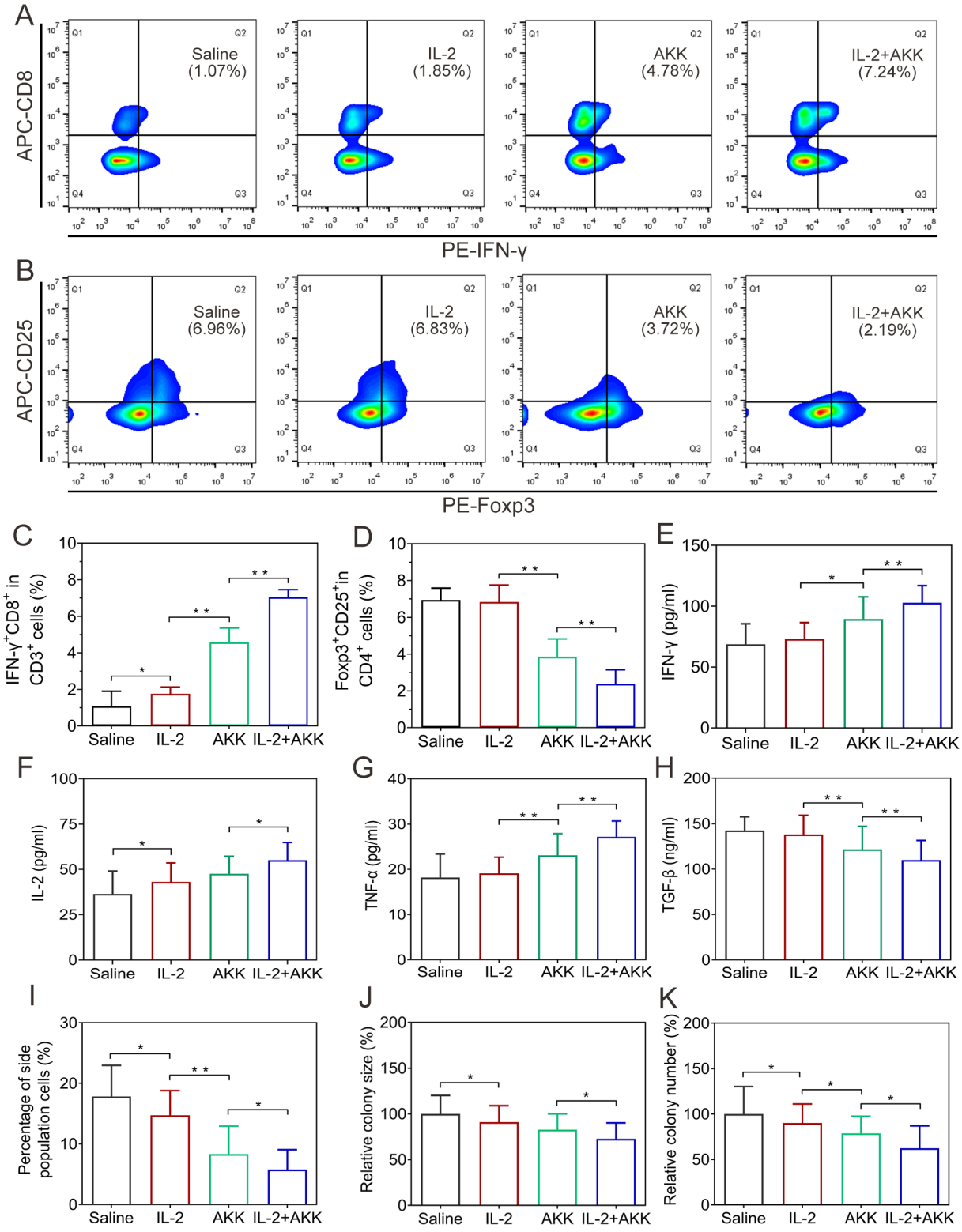

Figure 4 Alterations of tumor immune microenvironment in CT26 tumor-bearing mice receiving combination therapy of IL-2 and AKK. (A) Representative flow cytometry analysis of CTLs in tumor-draining lymph nodes. (B) Representative flow cytometry analysis of Tregs in tumor-draining lymph nodes. (C, D) Proportions of IFN-γ$^+$ CD8$^+$ in CD3$^+$ T cells (C) and Foxp3$^+$ CD25$^+$ in CD4$^+$ T cells (D). (E–H) ELISA measurement of IFN-γ (E) and IL-2 (F) in the homogenates of tumor tissues. ELISA measurement of TNF-α (G) and TGF-β (H) in the serum. (I) Percentage of side population cells in tumor tissues of B16F10 tumor-bearing mice at the end of tumor growth inhibition experiments. (J, K) Relative colony size (J) and number (K) of tumor spheroids on the fifth day after the tumor cells were seeded into the soft 3D fibrin gels. The tumor cells were collected and digested from tumor tissues of CT26 tumor-bearing mice receiving different treatments. All data are shown as mean±SD (n=6) (*p<0.05, **p<0.01). AKK, *Akkermansia muciniphila*; APC, allophycocyanin; IFN, interferon; IL-2, interleukin-2; TGF-β, transforming growth factor-β; TNF-α, tumor necrosis factor-α.

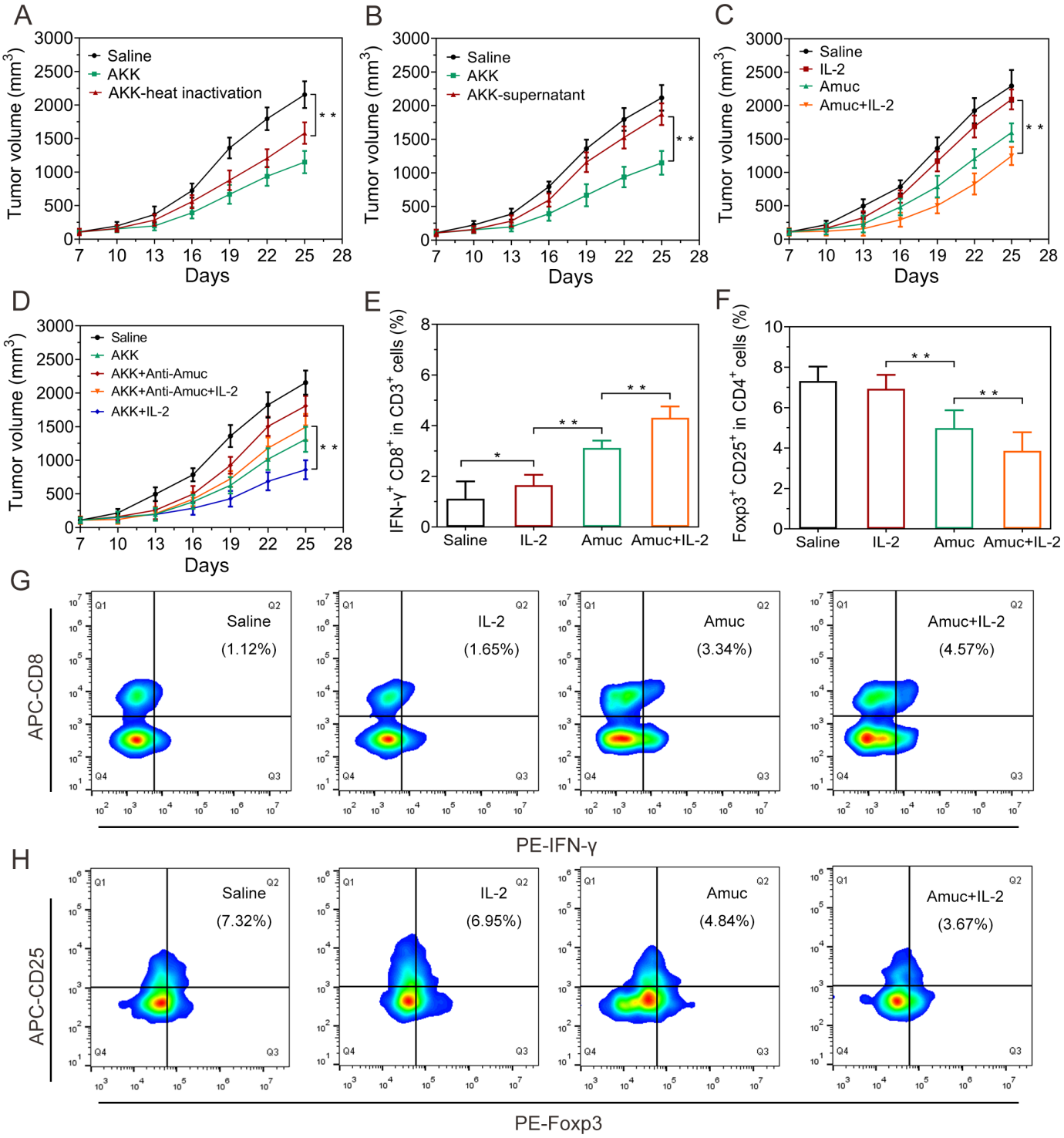

Figure 5 Antitumor effects of Amuc and its combination with IL-2 in CT26 tumor-bearing mice. (A) Tumor growth in mice treated with the pasteurized AKK. (B) Tumor growth in mice treated with the culture supernatant of AKK. (C) Tumor growth in mice treated with IL-2 and Amuc. (D) Tumor growth in mice treated with IL-2 and AKK bound with Amuc-specific antibody. (E) Proportions of IFN-γ$^+$ CD8$^+$ in CD3$^+$ T cells in tumor-draining lymph nodes. (F) Proportions of Foxp3$^+$ CD25$^+$ in CD4$^+$ T cells in tumor-draining lymph nodes. (G) Representative flow cytometry analysis of the CTLs in tumor-draining lymph nodes. (H) Representative flow cytometry analysis of Tregs in tumor-draining lymph nodes. All data are shown as mean±SD (n=6) (*p<0.05, **p<0.01). AKK, *Akkermansia muciniphila*; APC, allophycocyanin; CTL, cytotoxic T lymphocyte; IFN, interferon; IL-2, interleukin-2.

performed on the identified differentially expressed genes. The 10 most significantly enriched pathways were shown in figure 6B. Notably, the pathways of T helper cell differentiation, T cell receptor signaling, toll-like receptor (TLR) signaling and nuclear factor-κB (NF-κB) signaling pathway were clearly enriched in the

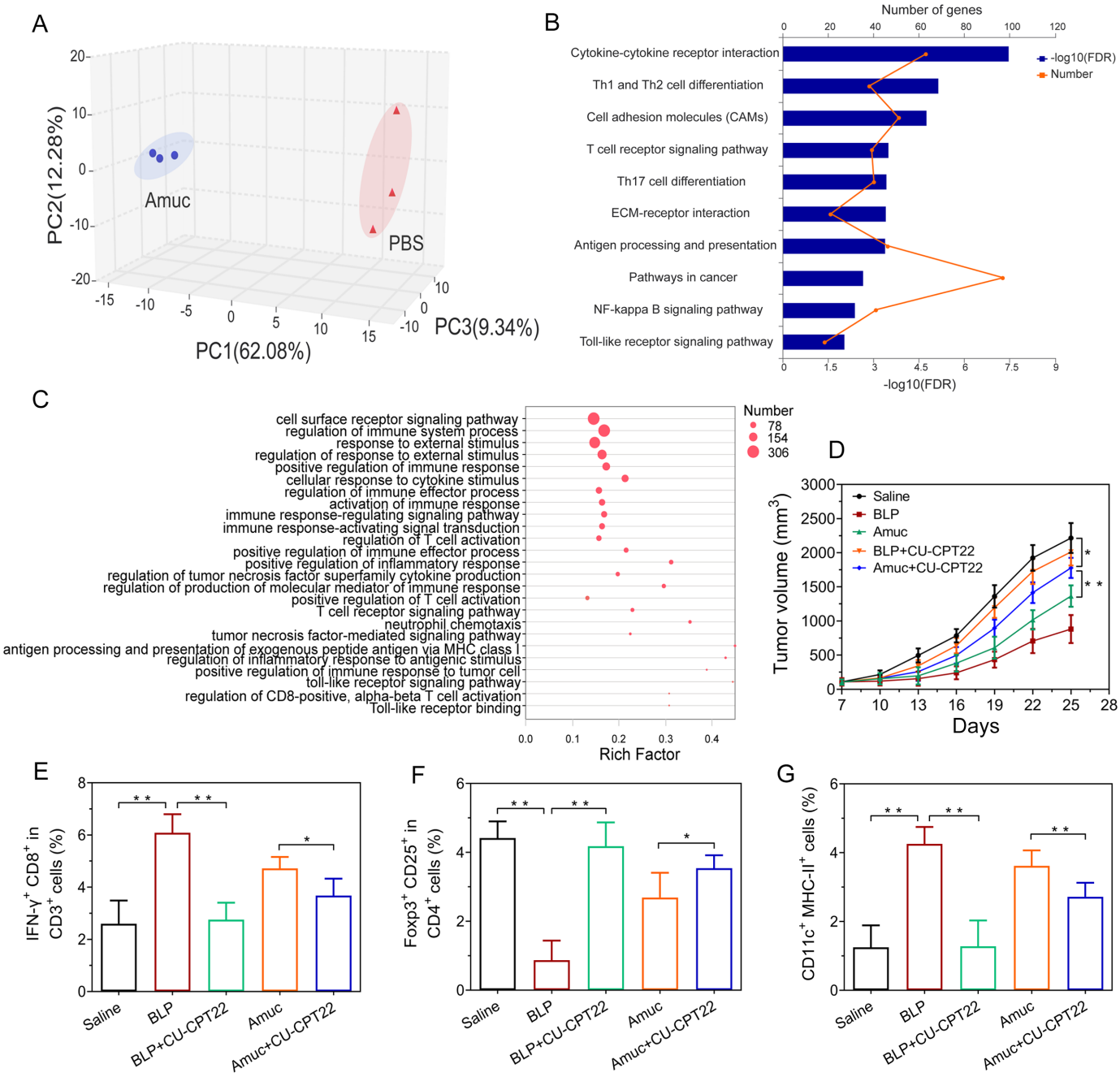

Figure 6 Mechanism study of Amuc in inducing antitumor-specific immune responses. (A–C) The involvement of immune responses in the tumor-infiltrating lymphocytes treated with Amuc. (A) 3D-principal coordinate analysis (3D-PCoA) analysis of the gene expression profiles. (B) Kyoto Encyclopedia of Genes and Genomes (KEGG) pathway enrichment analysis of the identified differentially expressed genes. (C) Gene ontology (GO) enrichment analysis of the identified differentially expressed genes involved in the immune functions. (D–G) The involvement of TLR2 pathway in the antitumor effects of Amuc in tumor-bearing mice, BLP acts as a TLR1/TLR2 agonist while CU-CPT22 acts as a TLR1/TLR2 antagonist. (D) Tumor growth under different treatment in CT26 tumor-bearing mice (n=6). (E) The proportions of IFN-γ^+ $CD8^+$ in $CD3^+$ T cells in tumor-draining lymph nodes. (F) The proportions of $Foxp3^+$ $CD25^+$ in $CD4^+$ T cells in tumor-draining lymph nodes. (G) The proportions of $CD11c^+$ $MHC\text{-}II^+$ cells in tumor-draining lymph nodes. All data are shown as mean±SD (*p<0.05, **p<0.01). BLP, bacterial lipoprotein; ECM, extracellular matrix; FDR, false discovery rate; IFN, interferon; MHC, major histocompatibility complex; NF-κB, nuclear factor-κB; PBS, phosphate-buffered saline; TLR2, toll-like receptor 2.

alteration of expressed genes induced by Amuc treatment (figure 6B). Furthermore, gene ontology (GO) enrichment analysis (figure 6C) showed that these differential genes were associated with the regulation of immune response, immune response-regulating signaling pathway, the regulation of T cell activation, TLR signaling pathway, and so on. These results indicate that the interaction between immune cells and Amuc may contribute to the Amuc-mediated antitumor efficacy.

Previous reports revealed that AKK specifically activated TLR2-expressing cells partly via Amuc.[24 25] The results of dual-luciferase reporter gene assay in TLR2-expressing HEK 293 T cells confirmed that Amuc activated the TLR2 pathway in a manner similar with AKK (online supplemental figure S21). To further explore the proposed mechanism of Amuc in regulating antitumor immune response in vivo, a synthetic bacterial lipoprotein (BLP, a TLR1/TLR2 agonist) and CU-CPT22 (a TLR1/TLR2 antagonist) were administrated to the tumor-bearing mice as a positive control and a negative control, respectively.[26] Amuc treatment generated antitumor effects similar with BLP treatment in tumor-bearing mice, and its combination with CU-CPT22 treatment resulted in impaired antitumor effects, suggesting that Amuc induces the tumor regression partly through TLR2 pathway (figure 6D and online supplemental figure S22). Notably, the alterations of the tumor microenvironment by Amuc were also regulated through the TLR2 pathway (figure 6E–G and online supplemental figure S23). TLR2 is also expressed on the surface of DCs.[27 28] DCs are potent professional antigen-presenting cells that can prime naive $CD8^+$ cells to induce the antigen-specific cytotoxic T cells.[28] The ex vivo immunostimulatory experiment showed that bone marrow-derived dendritic cells were activated by Amuc treatment probably through TLR2 pathway (online supplemental figure S24).

Enhancement of AKK on intestinal barrier integrity and gut microbiota homeostasis in the context of systemic IL-2 treatment

Combined treatment with IL-2 and AKK neither induced obvious body weight loss nor impaired liver function and white blood cell in B16F10 and CT26 tumor-bearing mice (online supplemental figure S25). In addition, neither morphological nor pathological damage is observed in H&E staining of the major tissues among each group (online supplemental figures S26, S27), suggesting that this combination therapy did not cause obvious toxicity in normal tissues. Histopathological analysis of intestine samples showed that IL-2 treatment exerted a significant adverse influence on gastrointestinal tract. As illustrated by H&E and periodic acid Schiff (PAS) staining, IL-2 treatment resulted in fewer intact intestinal villi and goblet cells, which indicated the damage of the intestinal mucosal barrier (figure 7A). In mice treated with IL-2, AKK supplementation was able to maintain intestinal morphology, thereby providing an intact mucosal barrier against infection and colitis.

Changes in the structure of the gut microbiota were visualized by 3D- PCoA analysis, revealing that the overall bacteria community of the combined treatment group gradually deviated from the saline treatment or IL-2 treatment alone (figure 7B). Oral administration of AKK also increased the richness of gut microbiota (figure 7C,D) in the IL-2-treated tumor-bearing mice. Moreover, the relative abundance of microbial community at genus level was changed by AKK treatment in the context of IL-2-based immunotherapy (online supplemental figure S28A). AKK supplementation dramatically increased the relative abundance of *Akkermansia*, *Allstipes* and *Lactobacillus* in IL-2-treated tumor-bearing mice. Besides, the correlations between *Akkermansia* and the level of tumor infiltration CTLs or Tregs (online supplemental figure S28B,C) were also testified, indicating that the relative abundance of AKK was in a positive correlation with the antitumor immune responses but in a negative correlation with immunosuppressive Treg responses.

DISCUSSION

There has been increasing research focusing on the interaction between the intrinsic immunological capacity and tumor cells in the tumor microenvironment.[29] Immunotherapies, including immune checkpoint blockades and IL-2, boost antitumor-specific immune responses to fight against cancer.[9 30] Meanwhile, gut commensal bacteria has been proven to play important roles in modulating host immune functions and influencing the response to cancer immunotherapies among patients.[31 32] In our previous works and others, improved anticancer efficiencies have been demonstrated by combined administration of immune therapeutics including checkpoint blockades or TGF-β inhibitors with commensal probiotics.[33 34] Because there are huge varieties of commensal bacteria in the intestine and different kinds of immune therapeutics, their relationship in cancer treatment is still far from clarified.[35] Furthermore, the molecular mechanism underlying such combination has rarely been studied.[21] Therefore, in the present study, the antitumor effect of IL-2 combined with AKK was investigated in ex vivo tumor tissues from patients with CRC and tumor-bearing mouse models.

Cytokines are small glycoproteins binding to cell surface receptors to regulate the development and function of immune cells and serve as potential therapeutic agents in cancer treatment.[36] IL-2 is a well-known immunostimulatory cytokine, which is identified as 'T-cell growth factor' and has revolutionized the fields of basic immunology research and cancer immunotherapy.[10 37] However, due to the diversity of the targeted cells, there is always a trade-off between therapeutic efficiency and adverse effects in the context of IL-2-based treatment.[8 38] In addition, patients undergoing IL-2 therapy showed limited efficacy due to the insufficient induction of CTLs and the expansion of immunosuppressive Tregs in some cases.[10 37] We found that IL-2 increased the proportion of CTLs, but showed limited effect on immunosuppressive Treg cells in either ex vivo tumor tissues from patients with CRC or tumor-bearing mice. These results were in line with other previous findings.[39 40] Thus, combination with other therapeutic approaches is necessary to further improve the efficacy of IL-2.

In the present study, oral administration of AKK alone induced tumor shrinkage and prolonged the median survival compared with IL-2 injection alone in tumor-bearing mice, which resulted from eliciting the

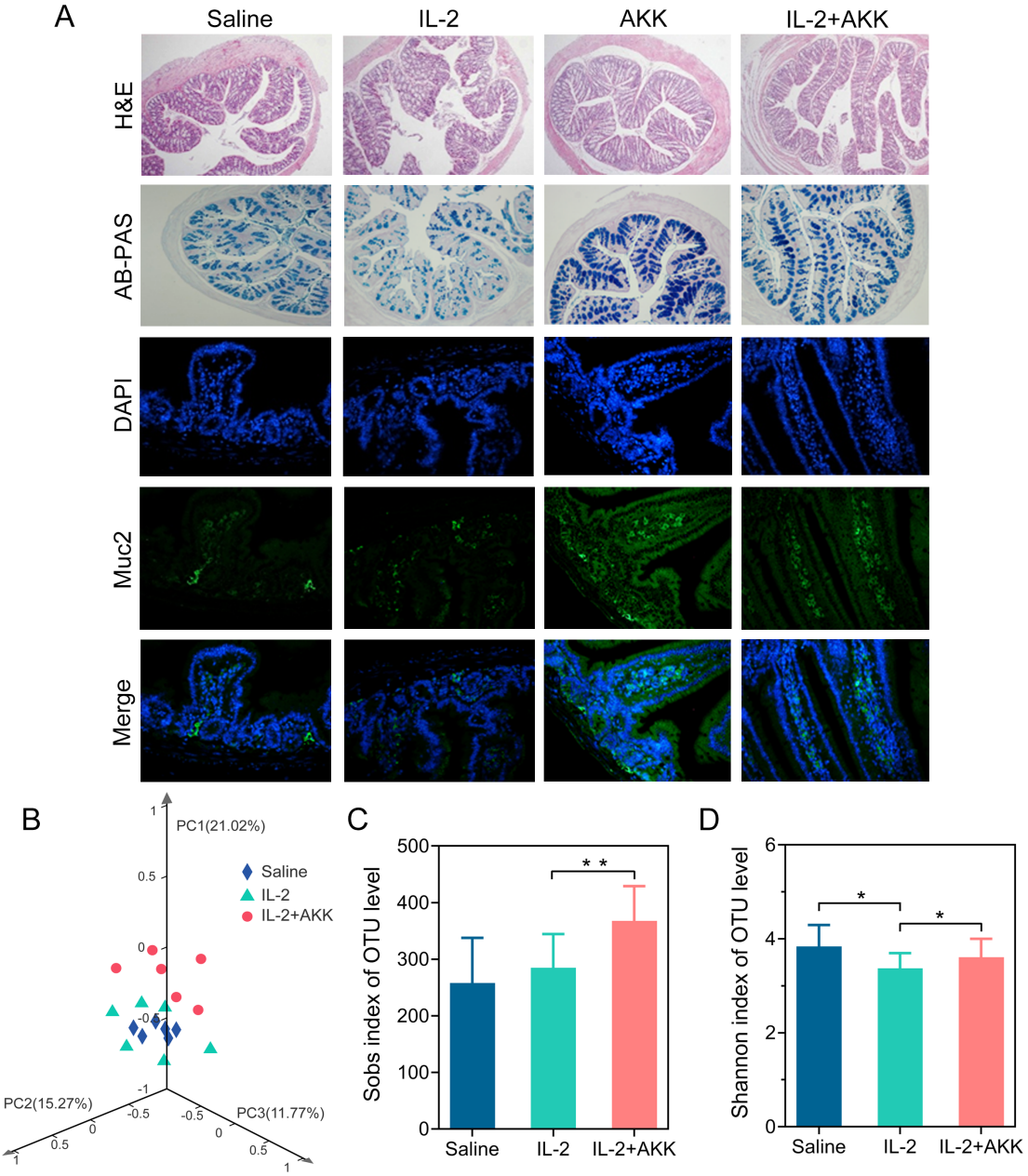

Figure 7 Oral administration of AKK improved gut barrier function and commensal microbiota homeostasis under IL-2 treatment in tumor-bearing mice. (A) Representative images of H&E and AB-PAS staining of the colon tissues and immunofluorescence staining of the mucus in the small intestine. (B) 3D-Principal coordinate analysis (3D- PCoA) of fecal samples (Bray-Curtis distances), followed by Adonis test (*p<0.05). (C) Observed richness (Sobs) index. (D) Shannon diversity index. All data are shown as mean±SD (n=6) (*p<0.05, **p<0.01). AB-PAS, alcian blue-periodic acid Schiff; AKK, *Akkermansia muciniphila;* DAPI, 4',6-diamidino-2-phenylindole; IL-2, interleukin 2; OTU, operational taxonomic unit.

antitumor immune response rather than directly killing the tumor cells (online supplemental figure S29). In particular, it was found that preadministration with AKK alone recruited a higher proportion of CTLs and produced a higher level of IFN-γ in tumor mass as well as TNF-α level in the serum in tumor-bearing mice, which were consistent with other studies.[41] Meanwhile, AKK treatment could also effectively decrease the ratio of Treg cells in tumor microenvironment and reduce the level of immunosuppressive cytokine TGF-β in the serum. More importantly, IL-2 treatment in combination with AKK elicited stronger efficacy in regulating Tregs or TGF-β level compared with single treatments (figure 4D,H). These synergistic effects partly contribute to the enhanced antitumor immune responses of the combined therapy. These findings indicate the potential of AKK supplementation as an adjuvant strategy to boost the therapeutic response to IL-2. Our results are consistent with the accumulating evidence that AKK is associated with favorable antitumor immmunosurveillance and thereby contributes to the therapeutic efficacy

of tumor immunotherapies in both preclinical tumor models and patients with cancer.[12 13 21]

In addition to the alterations of vascular permeability, digestive symptoms such as diarrhea and vomiting sometimes emerged in patients receiving IL-2 treatment.[38 39] In our present study, colonic tissues from the IL-2-treated mice showed significant epithelial injury and mucus layer depletion compared with the tumor-bearing control. Moreover, IL-2 treatment disturbed the intestinal homeostasis. Intestinal mucus is secreted by intestinal goblet cells and plays an important role in maintaining intestinal mucosal barrier and resisting invasion of harmful substances.[16] AKK has been proven to stimulate host mucin production and acts as the gatekeeper of the mucosa to strengthen the intestinal barrier function.[18 20] Our results also revealed that oral administration of AKK could protect the IL-2-treated tumor-bearing mice from mucus layer loss. Besides, we used the strain-specific primer through PCR-based detection system to detect the presence of AKK in tumor-bearing mice after oral administration (online supplemental figures S30, S31). Results showed that the abundance of AKK was significantly enriched in both the fecal and the intestinal samples instead of tumor tissues, which was consistent with the results of 16S rRNA gene sequencing. Oral administration of AKK in the context of IL-2 systemic injection reflected an altered and enriched microbial community diversity, which were identified as the responsible modulator positively associated with the enhanced antitumor-specific immune response.

Despite the gradually recognized roles of AKK in antitumor immunosurveillance and its contribution to the therapeutic efficacy of tumor immunotherapies,[1 13] the exact mechanism behind tumor regression and immune surveillance elicited by AKK is still far from elucidated. Due to the oxygen tolerance of AKK under ex vivo experiment conditions (online supplemental figure S32) and the maintained antitumor immune responses elicited by pasteurized AKK (figure 5A), it is hypothesized that the immune responses may partly mediate by its extracellular proteins with unique antigenic epitopes. In previous studies, the outer membrane protein of AKK contributed to the effects of AKK in controlling body weight, preventing obesity and the associated metabolic disorders.[20 24 25] Intriguingly, our study revealed that the antitumor immune response induced by AKK was closely related to its outer membrane protein, Amuc. Stimulating antitumor immune response rather than directly killing tumor cells was involved in the tumor inhibitory effect of Amuc. Besides, IL-2 treatment in combination with Amuc also triggered better tumor suppression compared with single treatment in both tumor-bearing mice models, which is consistent with the combined treatment of IL-2 and AKK. Due to the paralleled antitumor effect between AKK and Amuc, further exploration of the potential targets of Amuc helps to elucidate the molecular mechanism of AKK in tumor regression. Through RNA-sequencing analysis, we found that Amuc was closely related to T cell-mediated antitumor immune response, particularly by activation of TLR signal and NF-κB signaling pathways. Mounting evidences confirmed that certain TLR agonists were able to delay tumor growth through remodeling CTLs and Tregs function in cancer immunotherapy.[42 43] Here, in tumor-bearing mice, it was first found that tumor suppression efficacy of Amuc was partly mediated through TLR2 signaling pathway, which is consistent with other reports that activation of TLR2 was capable of remodeling tumor immune microenvironment and, in turn, inducing significant tumor shrink.[44–48] In addition, our results are also in line with the previous studies that Amuc could specially stimulate ex vivo TLR2-expressing cells to prevent the development of obesity and type 2 diabetes.[24]

As an active part of AKK to produce antitumor effects, Amuc can also be used as a potential adjuvant for cancer immunotherapy. In addition to oral administration, in situ injection of Amuc resulted in significant tumor regression (online supplemental figure S33) without significant body weight loss (online supplemental figure S34) in both tumor-bearing mice. Furthermore, abscopal effects were induced by local injection of Amuc (online supplemental figure S35), indicating that the systemic tumor-specific immune responses were involved under Amuc treatment. Therefore, Amuc, delivered by either oral or parenteral route, can be used as a potential adjuvant for cancer immunotherapy and worth further development in clinical translational research.

The challenges ahead should be noted that the antitumor immune response of AKK may follow other ways beyond Amuc involved and TLR2 mediated. Besides, there is still a need for further research and exploration on the roles of other commensal bacteria in the context of IL-2-based immunotherapy. Therefore, devoting more efforts to exploring the interindividual heterogeneity of microbiota community in preclinical models and clinical practice would provide new insights into cancer immunotherapy.

CONCLUSION

In summary, our results provide evidences that the specific commensal strain AKK was able to reinforce the therapeutic efficacy of IL-2-based immunotherapy. Combined treatment with IL-2 and AKK could generate a better tumor control, which was accompanied by recruiting more tumor-specific CTLs and decreasing immunosuppressive Tregs within the tumor microenvironment. The antitumor immune response induced by AKK was likely attributed to its outer membrane protein Amuc through activating TLR2 signaling and thus acquired effective tumor regression. Hence, our findings provide a more comprehensive insights to restore the efficacy of IL-2-based immunotherapy through precisely manipulating the gut microbiota among patients with cancer.

Author affiliations
[1]National Engineering Research Center for Nanomedicine, College of Life Science and Technology, Huazhong University of Science and Technology, Wuhan, China
[2]Department of Biotechnology, College of Life Science and Technology, Huazhong University of Science and Technology, Wuhan, China
[3]Hepatic Surgery Center, Tongji Hospital, Tongji Medical College, Huazhong University of Science and Technology, Wuhan, China
[4]Department of Biology, St. Olaf College, Northfield, Minnesota, USA

Acknowledgements We are very grateful to the patients and mice for their contributions to this study. We thank the technical support of Dr Shuyan Liang and Dr Zhixin Qiu from Wuhan Biobank Co, and Dr Min Lei from the Core Facilities for Life Science Research, Huazhong University of Science and Technology.

Contributors LS performed the experiments and prepared the manuscript. JS contributed to study design and drafted the manuscript. GC, CS and BL assisted in in vivo experiments. PZ contributed to sample collections and study design. CP and JW contributed to manuscript review. BZ, ZL and XY supervised the study and provided the overall guidance. The authors read and approved the final manuscript.

Funding This work was supported by grants from National Key Research and Development Project of China (2019YFA0905600), National Basic Research Program of China (2015CB931802 and 2018YFA0208903), National Natural Science Foundation of China (81627901, 81703443 and 81773653).

Competing interests None declared.

Patient consent for publication Not required.

Ethics approval All patients with CRC were diagnosed by pathologists and provided written informed consent prior to study enrollment. This study was approved by the Clinical Research Ethics Committee of Tongji Hospital, Huazhong University of Science and Technology and performed in accordance with the Helsinki Declaration. All mice received the humane care and the experimental protocols were carried out in accordance with the Guide for the Care and Use of Laboratory Animals, Huazhong University of Science and Technology, as approved by the Animal Care Committee of Hubei Province.

Provenance and peer review Not commissioned; externally peer reviewed.

Data availability statement Data are available upon reasonable request. All data relevant to the study are included in the article or uploaded as supplementary information. All data relevant to this study are included in this article or uploaded as online supplementary information. Data are available upon reasonable request.

ORCID iDs
Jianyong Sheng http://orcid.org/0000-0003-2363-1609
Zhi Liu http://orcid.org/0000-0002-8695-9276

REFERENCES

1 Ren D, Hua Y, Yu B, *et al*. Predictive biomarkers and mechanisms underlying resistance to PD1/PD-L1 blockade cancer immunotherapy. *Mol Cancer* 2020;19:19.
2 Yi M, Jiao D, Xu H, *et al*. Biomarkers for predicting efficacy of PD-1/PD-L1 inhibitors. *Mol Cancer* 2018;17:129.
3 Lizée G, Overwijk WW, Radvanyi L, *et al*. Harnessing the power of the immune system to target cancer. *Annu Rev Med* 2013;64:71–90.
4 Pitt JM, Vétizou M, Daillère R, *et al*. Resistance mechanisms to Immune-Checkpoint blockade in cancer: tumor-intrinsic and -Extrinsic factors. *Immunity* 2016;44:1255–69.
5 Das S, Johnson DB. Immune-Related adverse events and anti-tumor efficacy of immune checkpoint inhibitors. *J Immunother Cancer* 2019;7:306.
6 Boutros C, Tarhini A, Routier E, *et al*. Safety profiles of anti-CTLA-4 and anti-PD-1 antibodies alone and in combination. *Nat Rev Clin Oncol* 2016;13:473–86.
7 Malek TR. The biology of interleukin-2. *Annu Rev Immunol* 2008;26:453–79.
8 Dhupkar P, Gordon N. Interleukin-2: old and new approaches to enhance Immune-Therapeutic efficacy. *Adv Exp Med Biol* 2017;995:33–51.
9 Sim GC, Radvanyi L. The IL-2 cytokine family in cancer immunotherapy. *Cytokine Growth Factor Rev* 2014;25:377–90.
10 Jiang T, Zhou C, Ren S. Role of IL-2 in cancer immunotherapy. *Oncoimmunology* 2016;5:e1163462.
11 Nelson MH, Diven MA, Huff LW, *et al*. Harnessing the microbiome to enhance cancer immunotherapy. *J Immunol Res* 2015;2015:1–12.
12 Zheng Y, Wang T, Tu X, *et al*. Gut microbiome affects the response to anti-PD-1 immunotherapy in patients with hepatocellular carcinoma. *J Immunother Cancer* 2019;7:193.
13 Routy B, Le Chatelier E, Derosa L, *et al*. Gut microbiome influences efficacy of PD-1-based immunotherapy against epithelial tumors. *Science* 2018;359:91–7.
14 Vétizou M, Pitt JM, Daillère R, *et al*. Anticancer immunotherapy by CTLA-4 blockade relies on the gut microbiota. *Science* 2015;350:1079–84.
15 Yi M, Yu S, Qin S, *et al*. Gut microbiome modulates efficacy of immune checkpoint inhibitors. *J Hematol Oncol* 2018;11:47.
16 Routy B, Gopalakrishnan V, Daillère R, *et al*. The gut microbiota influences anticancer immunosurveillance and general health. *Nat Rev Clin Oncol* 2018;15:382–96.
17 Collado MC, Derrien M, Isolauri E, *et al*. Intestinal integrity and Akkermansia muciniphila, a mucin-degrading member of the intestinal microbiota present in infants, adults, and the elderly. *Appl Environ Microbiol* 2007;73:7767–70.
18 Derrien M, Belzer C, de Vos WM. Akkermansia muciniphila and its role in regulating host functions. *Microb Pathog* 2017;106:171–81.
19 Zhang T, Li Q, Cheng L, *et al*. Akkermansia muciniphila is a promising probiotic. *Microb Biotechnol* 2019;12:1109–25.
20 Everard A, Belzer C, Geurts L, *et al*. Cross-Talk between Akkermansia muciniphila and intestinal epithelium controls diet-induced obesity. *Proc Natl Acad Sci U S A* 2013;110:9066–71.
21 Fessler J, Matson V, Gajewski TF. Exploring the emerging role of the microbiome in cancer immunotherapy. *J Immunother Cancer* 2019;7:108.
22 Ma J, Zhang Y, Tang K, *et al*. Reversing drug resistance of soft tumor-repopulating cells by tumor cell-derived chemotherapeutic microparticles. *Cell Res* 2016;26:713–27.
23 Sun Y, Zheng Zu'an, Zhang H, *et al*. Chemotherapeutic tumor microparticles combining low-dose irradiation reprogram tumor-promoting macrophages through a tumor-repopulating cell-curtailing pathway. *Oncoimmunology* 2017;6:e1309487.
24 Plovier H, Everard A, Druart C, *et al*. A purified membrane protein from Akkermansia muciniphila or the pasteurized bacterium improves metabolism in obese and diabetic mice. *Nat Med* 2017;23:107–13.
25 Depommier C, Everard A, Druart C, *et al*. Supplementation with Akkermansia muciniphila in overweight and obese human volunteers: a proof-of-concept exploratory study. *Nat Med* 2019;25:1096–103.
26 Adams S. Toll-Like receptor agonists in cancer therapy. *Immunotherapy* 2009;1:949–64.
27 Huang L, Xu H, Peng G. Tlr-Mediated metabolic reprogramming in the tumor microenvironment: potential novel strategies for cancer immunotherapy. *Cell Mol Immunol* 2018;15:428–37.
28 Wu H-J, Wu E. The role of gut microbiota in immune homeostasis and autoimmunity. *Gut Microbes* 2012;3:4–14.
29 Whiteside TL. The tumor microenvironment and its role in promoting tumor growth. *Oncogene* 2008;27:5904–12.
30 Topalian SL. Targeting immune checkpoints in cancer therapy. *JAMA* 2017;318:1647–8.
31 Pope JL, Tomkovich S, Yang Y, *et al*. Microbiota as a mediator of cancer progression and therapy. *Transl Res* 2017;179:139–54.
32 Li J, Sung CYJ, Lee N, *et al*. Probiotics modulated gut microbiota suppresses hepatocellular carcinoma growth in mice. *Proc Natl Acad Sci U S A* 2016;113:E1306–15.
33 Shi L, Sheng J, Wang M, *et al*. Combination therapy of TGF-β blockade and Commensal-derived probiotics provides enhanced antitumor immune response and tumor suppression. *Theranostics* 2019;9:4115–29.
34 Sivan A, Corrales L, Hubert N, *et al*. Commensal Bifidobacterium promotes antitumor immunity and facilitates anti-PD-L1 efficacy. *Science* 2015;350:1084–9.
35 Gopalakrishnan V, Helmink BA, Spencer CN, *et al*. The influence of the gut microbiome on cancer, immunity, and cancer immunotherapy. *Cancer Cell* 2018;33:570–80.
36 Waldmann TA. Cytokines in cancer immunotherapy. *Cold Spring Harb Perspect Biol* 2018:10.

37 Liao W, Lin J-X, Leonard WJ. Il-2 family cytokines: new insights into the complex roles of IL-2 as a broad regulator of T helper cell differentiation. *Curr Opin Immunol* 2011;23:598–604.
38 Skrombolas D, Frelinger JG. Challenges and developing solutions for increasing the benefits of IL-2 treatment in tumor therapy. *Expert Rev Clin Immunol* 2014;10:207–17.
39 Liao W, Lin J-X, Leonard WJ. Interleukin-2 at the crossroads of effector responses, tolerance, and immunotherapy. *Immunity* 2013;38:13–25.
40 Park J, Wrzesinski SH, Stern E, *et al*. Combination delivery of TGF-β inhibitor and IL-2 by nanoscale liposomal polymeric gels enhances tumour immunotherapy. *Nat Mater* 2012;11:895–905.
41 Cekanaviciute E, Yoo BB, Runia TF, *et al*. Gut bacteria from multiple sclerosis patients modulate human T cells and exacerbate symptoms in mouse models. *Proc Natl Acad Sci U S A* 2017;114:10713–8.
42 Feng Y, Mu R, Wang Z, *et al*. A Toll-like receptor agonist mimicking microbial signal to generate tumor-suppressive macrophages. *Nat Commun* 2019;10:2272.
43 Smith M, García-Martínez E, Pitter MR, *et al*. Trial watch: Toll-like receptor agonists in cancer immunotherapy. *Oncoimmunology* 2018;7:e1526250.
44 Zhang Y, Luo F, Cai Y, *et al*. Tlr1/Tlr2 agonist induces tumor regression by reciprocal modulation of effector and regulatory T cells. *J Immunol* 2011;186:1963–9.
45 Cen X, Zhu G, Yang J, *et al*. TLR1/2 specific small-molecule agonist suppresses leukemia cancer cell growth by stimulating cytotoxic T lymphocytes. *Adv Sci* 2019;6:1802042.
46 Lu H, Yang Y, Gad E, *et al*. TLR2 agonist PSK activates human NK cells and enhances the antitumor effect of HER2-targeted monoclonal antibody therapy. *Clin Cancer Res* 2011;17:6742–53.
47 Zom GG, Willems MMJHP, Khan S, *et al*. Novel TLR2-binding adjuvant induces enhanced T cell responses and tumor eradication. *J Immunother Cancer* 2018;6:146.
48 Zom GG, Khan S, Britten CM, *et al*. Efficient induction of antitumor immunity by synthetic Toll-like receptor ligand-peptide conjugates. *Cancer Immunol Res* 2014;2:756–64.

Supporting Information

Combining IL-2-based Immunotherapy with Commensal Probiotics Produces Enhanced Antitumor Immune Response and Tumor Clearance

Linlin Shi[1†], Jianyong Sheng[1†], Guozhong Chen[2], Peng Zhu[3], Changping Shi[2], Bei Li[2], Chaiwoo Park[2], Jingyi Wang[4], Bixiang Zhang[3*], Zhi Liu[2*] and Xiangliang Yang[1*]

[1]National Engineering Research Center for Nanomedicine, College of Life Science and Technology, Huazhong University of Science and Technology, Wuhan, China

[2]Department of Biotechnology, College of Life Science and Technology, Huazhong University of Science and Technology, Wuhan, China

[3]Hepatic Surgery Center, Tongji Hospital, Tongji Medical College, Huazhong University of Science and Technology, Wuhan, China

[4]Department of Biology, St. Olaf College, Minnesota, USA

[†] These author contributed equally to this work.

* Correspondence: bixiangzhang@163.com; zhiliu@hust.edu.cn; yangxl@hust.edu.cn

Inventory

Supplementary Materials and Methods

35 Supplementary Figures

1 Supplementary Table

Supplementary Materials and Methods

Flow cytometry analysis of CRC patients derived tumor tissues

Tumor tissues collected from CRC patients were cut into small pieces and digested and filtered into single cell suspensions. For cell viability analysis, IL-2 and AKK were prepared and added to the cultured cells from CRC patients. The cells were observed under a microscope every six hours. After cultured for 24 hours, cells were collected and stained with annexin V and propidiumiodide for apoptosis detection by flow cytometry. For tumor immune microenvironment analysis, single cell suspensions of tumor infiltrating lymphocytes were isolated from CRC patients and treated with IL-2, AKK and their combined therapy for 24h. For cell surface staining, the suspensions were incubated with FITC-labeled anti-human CD3 antibody (clone HIT3a, cat. 300306), PerCP/Cy5.5-labeled anti-human CD4 antibody (clone RPA-T4, cat. 300529) and PE-labeled anti-human CD8a antibody (clone RPA-T8, cat. 301008). For intracellular cytokine staining, lymphocytes prepared from tumor mass were restimulated using phorbol 12-myristate 13-acetate (PMA; 50 ng/mL) and ionomycin (1mg/mL; Sigma-Aldrich) in the presence of Brefeldin A (1 mg/mL; eBioscience) for 4h. Subsequently, the simulated lymphocytes were stained with FITC-labeled anti-mouse CD3 antibody and PE-labeled anti-human CD8a antibody as described above. After surface staining, cells were treated with Fix/Perm solution and restained with APC anti-human IFN-γ antibody (clone 4S.B3, cat. 502511). For dendritic cell analysis, tumor infiltrating lymphocytes were stained with APC-labeled anti-human CD11c antibody (clone 3.9, cat. 301613), PE-labeled anti-human I-A/I-E antibody (clone L243, cat. 307605), FITC-labeled anti-human CD80 antibody (clone 2D10, cat. 305205) and PerCP/Cy5.5-labeled anti-human CD86 antibody (clone IT2.2, cat. 305419).

Flow cytometry analysis of tumor-bearing mice derived tumor tissues

Tumor tissues were isolated from subcutaneous tumor bearing mice, digested by collagenase and filtered into single cell suspensions. Afterward, the suspensions were stained with FITC-labeled anti-mouse CD3 antibody (clone 145-2C11, cat. 100203), PerCP/Cy5.5-labeled anti-mouse CD4 antibody (clone GK1.5, cat. 100434) and APC-labeled anti-mouse CD8a antibody (clone 53-6.7, cat. 100712). For intracellular cytokine staining, single cell suspensions prepared from tumor infiltrating lymph node were restimulated using phorbol 12-myristate 13-acetate (PMA; 50 ng/mL) and ionomycin (1mg/mL; Sigma-Aldrich) in the presence of Brefeldin A (1 mg/ml; eBioscience) for 4h. Subsequently, the simulated lymphocytes were stained with FITC-labeled anti-mouse CD3 antibody and APC-labeled anti-mouse CD8a antibody as described above. After surface staining, cells were treated with Fix/Perm solution and restained with PE-labeled anti-mouse IFN-γ antibody (clone XMG1.2, cat. 505807). For nuclear transcription factor staining, tumor infiltrating lymphocyte were stained with PerCP/Cy5.5-labeled anti-mouse CD4 antibody and APC-labeled anti-mouse CD25 antibody (clone PC 61, cat. 102011). Afterwards, cells were incubated with Fix/Perm solution and restained with PE-labeled anti-mouse Foxp3 antibody (clone MF-14, cat. 126403). For dendritic cell analysis, tumor infiltrating lymphocytes were stained with FITC-labeled anti-mouse CD11c antibody (clone N418, cat. 117305), PE/Cy7-labeled anti-mouse I-A/I-E antibody (clone M5/114.15.2, cat. 107629), PE-labeled anti-mouse CD80 antibody (clone 16-10A1, cat. 104707) and APC-labeled anti-mouse CD86 antibody (clone GL-1, cat. 105011). All antibodies were purchased from BioLegend (San Diego, USA), and flow cytometric analysis was performed by using a CytoFlex flow cytometry system (Beckman Coulter, USA).

Flow cytometry analysis of side population cells

1×10^6 single cell suspensions in culture medium containing 1 % FBS were prepared from tumor tissues of subcutaneous tumor bearing mice. The suspensions were stained with fluorescent dye (Hoechst 33342) at 5 μg/mL in the presence or absence of 50 μM verapamil. Then, cells were

incubated in darkness at 37 °C for 90 min, washed twice with pre-cooling PBS and resuspended in 300 μL PBS and kept on ice until further analysis.

Tumor-repopulating cells culture

Tumor-repopulating cells were selected from the single cell suspensions by soft 3D fibrin gels according to the previous study [1]. First, fibrinogen was diluted to 2 mg/mL with T7 buffer (50 mM Tris, pH 7.4, 150 mM NaCl). Fibrinogen/cell mixtures were obtained by blending 2 mg/mL fibrinogen with similar volume of cell suspension (2×10^3 cells/mL), which produced gels of 90 Pa in elastic stiffness. 250 μL of the mixtures were loaded into each well of 24-well plate pre-added with 5 μL thrombin (0.1 U/μL). The cell culture plate was then incubated at 37 °C for 30 min. Finally, 1 ml RPMI 1640 medium containing 10 % FBS and antibiotics were added. On the fifth day, tumor spheroids were obtained, and the colony size and number were measured.

Antitumor effect and mechanism study of Amuc in tumor bearing mice

To explore the involvement of TLR2 pathway in the antitumor effects of Amuc, tumor-bearing mice received i.p. injection of BLP at 10 μg per mice and CU-CPT22 at 3 mg/kg every 5 days for 3 weeks. Amuc was delivered at 10 μg per mice by oral administration every three days for 3 weeks. Tumor volume and body weight were recorded every 3 days. The length (L) and width (W) of tumor were measured every other day with a digital caliper and tumor volume was calculated as $L\times W^2\times0.5$. When the tumor volume reached about 2000 mm^3, mice were sacrificed according to the guidelines for animal care. Tumor samples were collected for further analysis. All mice received the humane care and had free access to water and the maintenance diet.

Dual-luciferase reporter gene assay for TLR2

Human HEK 293T cells were seeded at a density of 1×10^5 cells in 24-well plates. Cells were transfected with 1μg PCDNA3.1(+)-hTLR2-Flag plasmid, 0.5 μg pGL4.32-NF-κB-luciferase

plasmid, and 0.01 ug pRL-TK plasmid by using Lipofectamine 2000 reagent (Invitrogen). After incubation for 24 h, the transfection solutions were replaced with AKK suspension (1×10^7 CFU/mL) or Amuc solution (10 μg/mL), followed by incubation at 37 °C in a 5% CO_2 incubator for 24 h. Receptor ligand Pam3CSK4 (10 ng/mL) and maintenance medium (DMEM) were used as the positive control and the negative control, respectively. Subsequently, cells were rinsed twice with PBS (pH 7.4) and lysed with 1× passive lysis buffer (100 μL/well). The Luciferase and Renilla luciferase activity were separately measured using a fluorescence spectrophotometer (GloMax® 20/20 Luminometer, Promega) following the manufacturer's instructions for the Dual-Luciferase Assay System (Promega). The activation ratio of TLR2/ NF-κB was calculated by fluorescent detection to evaluate the level of TLR2 activation.

AKK detection in vivo

Fecal samples, intestinal contents and tumor tissues were collected from saline treated tumor bearing mice and AKK treated mice. Total genomic DNA from the obtained samples were extracted by QIAamp DNA Stool Mini Kit and QIAamp Fast DNA Tissue Kit (QIAGEN, Germany) according to the manufacturer's guide. Specific primer sequences for the detection of AKK were chosen from the previous methods [2]. Samples were subjected to 35 cycles of amplification. Preincubation was for 5 min at 95 °C, followed by 35 cycles of 30 s at 95 °C, 30s at 54 °C, and 30 s at 72 °C. PCR products in each group were visualized by agarose gel electrophoresis following the standard protocols.

Microbial DNA extraction and sequencing

Mice fecal samples were frozen at -80 °C immediately after collection. Total genomic DNA from around 200 mg of stool was extracted by QIAamp DNA Stool Mini Kit (QIAGEN, Germany) according to the manufacturer's guide. The V3-V4 region of the bacterial 16S ribosomal RNA (rRNA) genes was amplified by PCR with universal primer sequences (338F, ACTCCTACGGGAGGCAGCAG; 806R, GGACTACHVGGGTWTCTAAT) and FastPfu Polymerase. Amplicons were then purified by gel extraction (AxyPrep DNA GelExtraction Kit,

Axygen Biosciences, USA) and were quantified using QuantiFluor-ST (Promega, USA). The purified amplicons were pooled in equimolar concentrations, and paired-end sequencing was performed using an Illumina MiSeq platform (Illumina, San Diego, USA).

Expression and purification of AKK-derived outer membrane protein

The outer membrane protein of AKK (here termed Amuc) was expressed and purified following the previous method with modifications [3]. The expression plasmid was constructed by amplification of its gene devoid of the coding sequence for its signal sequence and cloning of the resulting PCR product in pET28a-Amuc.

The resulted plasmid pET28a-Amuc, with the conformation confirmed by sequence analysis, was transformed into *E. coli* BL21. This strain was then grown in LB-broth containing kanamycin (50 μg/mL) followed by IPTG induction at a final concentration of 2 mM by shaking at 220 rpm at 28 °C. After ten hours of induction, cells were pelleted by centrifugation at 9,000 g for 15 min and stored at -80 °C for further lysis. Cell pellets were resuspended and lysed using lysozyme and ultrasonic homogenizer (SCIENTZ, Ningbo, China). After centrifugation, the supernatants were collected and purified for Amuc by using BeyoGold™ His-tag Purification Resin (Beyotime, Shanghai, China). The purified protein sample was determined by BCA assay and stored at -80 °C for further experiments.

RNA sequencing and data analysis

Total RNAs were prepared with Trizol reagent (Invitrogen, USA) and were sequenced by Illumina HiSeq X10 (Illumina, USA). Significance analysis (2-fold change and P-value < 0.05) was used to identify the differential genes with a false discovery rate (FDR) < 0.05. All identified sequences were mapped with Gene Ontology Terms (GO, http://geneontology.org/) and Kyoto Encyclopedia of Genes and Genomes (KEGG, https://www.kegg.jp/) to determine the functional and biological properties. Hypergeometric test was employed to conduct GO and KEGG pathway enrichment.

Preparation and purification of antibodies against Amuc

Polyclonal-antibodies against Amuc were prepared by Dia-An Biotech, China. 2 mg of purified Amuc protein was mixed with FCA (Freund's complete adjuvant) or FIA (Freund's incomplete adjuvant), followed by subcutaneous injection into two Japanese white rabbits for four times. The mixture containing FCA was only used in the first injection, while the mixture with FIA for the rest three injections. The 2nd injection was on the 28th day post the first injection. There were 2-week intervals between other injections. On the third day after the last injection, antiserum titer was tested by ELISA. On the 64th day post the first injection, the rabbits with higher titer was killed and its blood was collected. An affinity column for the purification of the antibodies was made by coupling 1mg purified Amuc protein to CNBr-activated Sepharose 4B from GE. The antiserum was applied onto the column, followed by elution of the specific antibodies using the Glycine HCl buffer at pH 2.5.

Culture and in vitro activation of BMDC

To prepare bone marrow-derived dendritic cells (BMDCs), the tibias and femurs of normal C57BL/6 mice (wt) were removed under sterile conditions. Bone marrow cells were flushed out from the bone cavity gently using the needle of a 1 mL syringe and then inserted into a sterile culture dish with RPMI-1640 medium. Cell suspensions in the dish were centrifuged at 1200 rpm for 5 min and resuspended in RPMI-1640 medium supplemented with 10% FBS, 10 ng/mL IL-4 and 20 ng/mL GM-CSF. Cell were then distributed into 24-well plates (NEST Biotechnology, Wuxi, China) at a density of 1×10^6 cell/mL and were cultured for 5 days in 37 °C, 5 % CO_2. On day 3, a fresh cell culture medium containing IL-4 and GM-CSF were added. On day 5, the nonadherent cells suspended in the medium were collected, centrifuged, and resuspended in the fresh culture medium containing IL-4 and GM-CSF. For further activation, 1×10^6 BMDCs were seeded in a 6-well plate (NEST Biotechnology, Wuxi, China) and stimulated with PBS, Amuc (10 μg/mL), and AKK (1×10^7 CFU/mL) for 24 h. The expression of the surface markers CD11c, MHC-II, and CD86 on the BMDCs was then measured and calculated by flow cytometry.

Histological analysis

Tumor tissues were fixed in 4 % paraformaldehyde, sectioned and stained with H&E. The rest of tumor tissues were frozen and prepared to be stained with Ki67 and TUNEL according to the manufacturer's instructions. Cell nuclei were stained by DAPI. For immunofluorescence staining of CD133, frozen slices of the dissected tumor tissues from different groups were blocked with 5% BSA in PBS for 60 min. Heat mediated antigen retrieval was performed in 0.01M citrate-buffer (pH 6.0). The slices were then incubated with a 1:500 dilution of anti-CD133 antibody (ab19898, Abcam, USA) and rocked on an orbital shaker (Mini Roller, NEST Biotechnology, China) at 4°C in the dark overnight. Afterwards the tumor slices were treated with CY3-conjugated goat anti-rabbit antibody (GB21303, Servicebio, China), the secondary antibody, in PBS at room temperature in the dark for 60 min. Cell nuclei were stained with DAPI (Sigma, USA). Stained cells were then visualized by fluorescence microscopy (Nikon Eclipse CI, Japan). Images were acquired with Nikon digital sight DS-Fi2 imaging system (exposure time: 10 ms for DAPI and 80 ms for CY3, at 200× magnification) under the same acquisition settings throughout image capturing. The positively stained cells were recorded from three visual fields at 200× magnification per slice. The average percentage of $CD133^+$ cells was processed using Image Pro Plus 6.0 (Media Cybernetics, USA).

Intestinal samples of mice were fixed in 4 % paraformaldehyde at room temperature overnight and then embedded in paraffin. Tissues were sectioned at 5 μm thickness and dipped in hematoxylin and eosin (H&E) using standard protocols. For AB-PAS staining, the mice intestinal samples were fixed in Carnoy's Fluid. Dewaxed sections were hydrated and stained with Alcian blue for 5-10 min followed by treatment with periodic acid for 10-15 min. Then, sections were stained with Schiff's reagent for 15-30 min in the darkness, washed in running tap water for 5-10 min and dehydrated in gradient alcohol before mounting with neutral gum. For immunofluorescent staining of mucus layer, intestinal samples of mice were stained with

Mucin2 (Santa Cruz Biotechnology, USA) following the standard procedures. Images of the stained sections were acquired by fluorescence microscopy (Nikon Eclipse CI, Japan).

References

1. Liu J, Tan Y, Zhang H, Zhang Y, Xu P, Chen J, Poh YC, Tang K, Wang N, Huang B. Soft fibrin gels promote selection and growth of tumorigenic cells. Nat Mater. 2012;11:734-41.
2. Collado MC, Derrien M, Isolauri E, de Vos WM, Salminen S. Intestinal integrity and Akkermansia muciniphila, a mucin-degrading member of the intestinal microbiota present in infants, adults, and the elderly. Appl Environ Microbiol. 2007; 73:7767-70.
3. Plovier H, Everard A, Druart C, Depommier C, Van Hul M, Geurts L, Chilloux J, Ottman N, Duparc T, Lichtenstein L, et al. A purified membrane protein from Akkermansia muciniphila or the pasteurized bacterium improves metabolism in obese and diabetic mice. Nat Med. 2017; 23:107-113.

Supplementary Figures

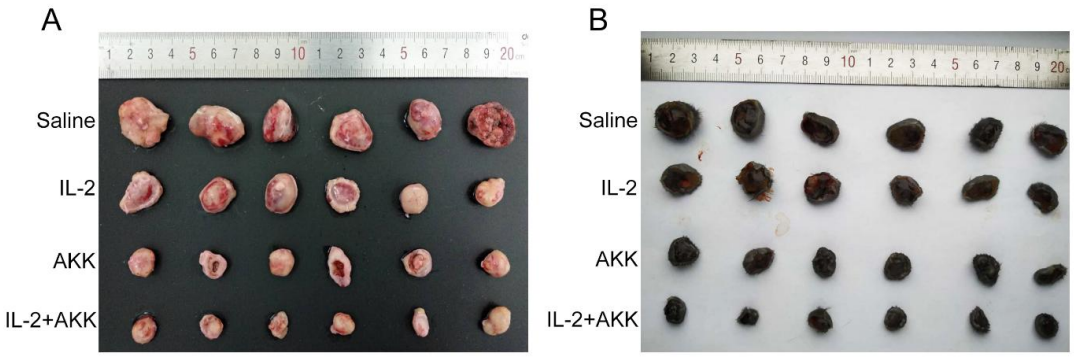

Figure S1. Antitumor effect of combination therapy of IL-2 and AKK in tumor bearing mice. Images of tumor tissues isolated from CT26 tumor-bearing mice (A) or B16F10 tumor-bearing mice (B) at the end of the experiment (n = 6).

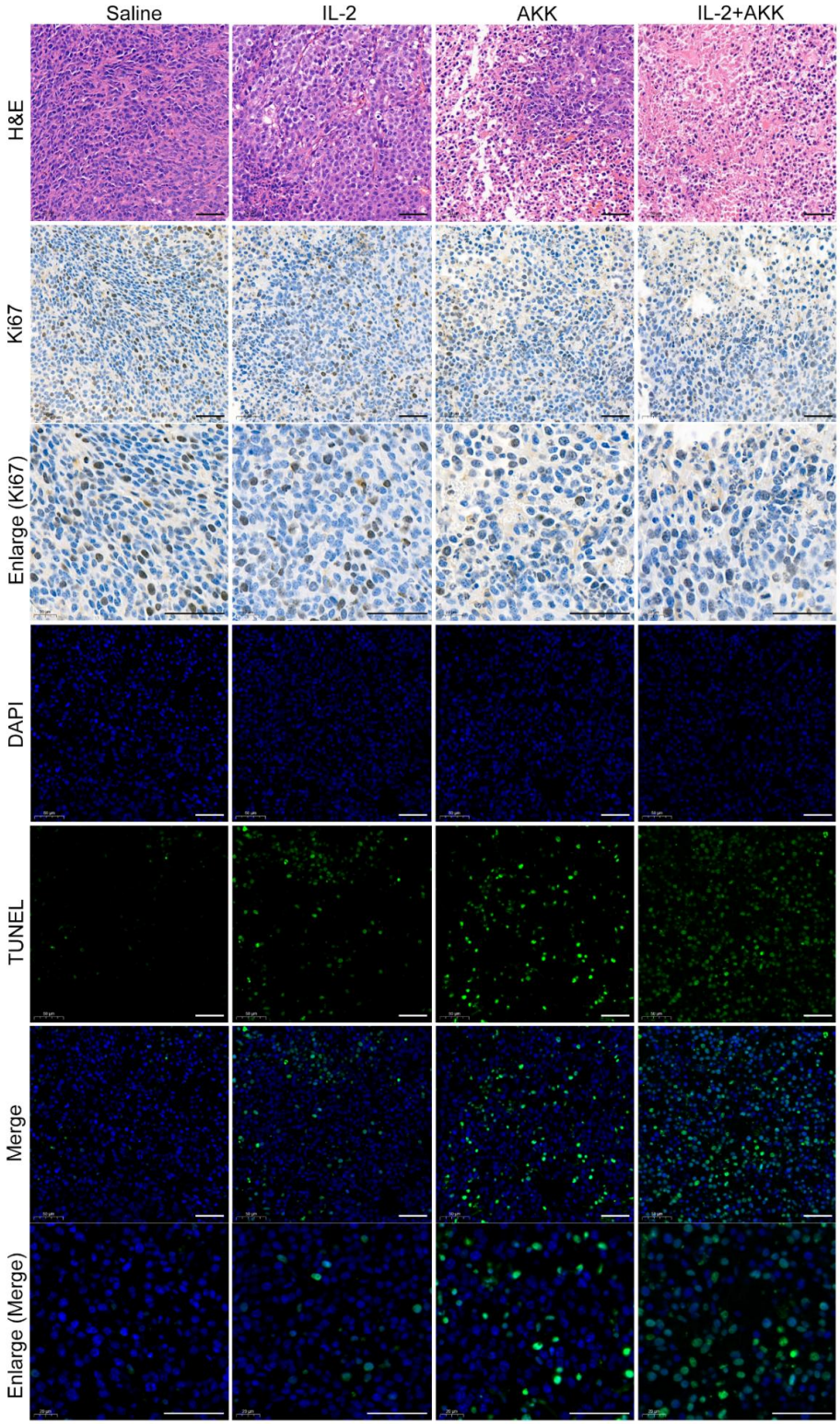

Figure S2. Representative histological staining of tumor sections from CT26 tumor-bearing mice at the end of the experiment (200× or 400× enlargement, scale bar = 50 μm).

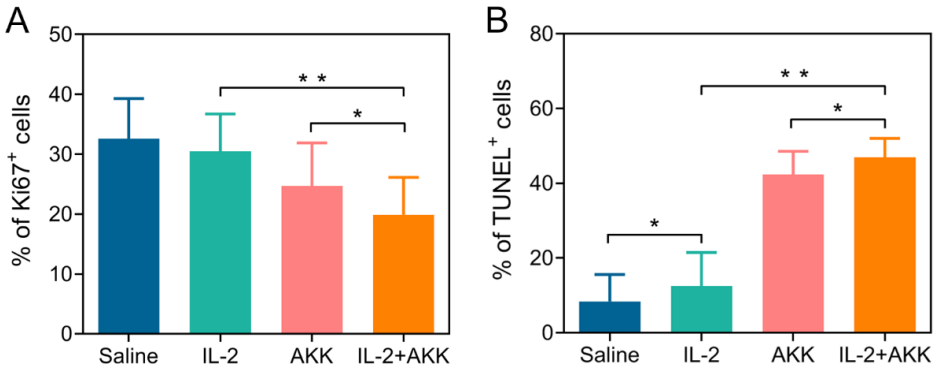

Figure S3. Quantitative analysis of Ki67$^+$ cells (A) and TUNEL$^+$ cells (B) in the tumor tissues collected from CT26 tumor bearing mice among different treatment groups (n = 6). All data are shown as mean ± SD (*$P < 0.05$, ** $P < 0.01$).

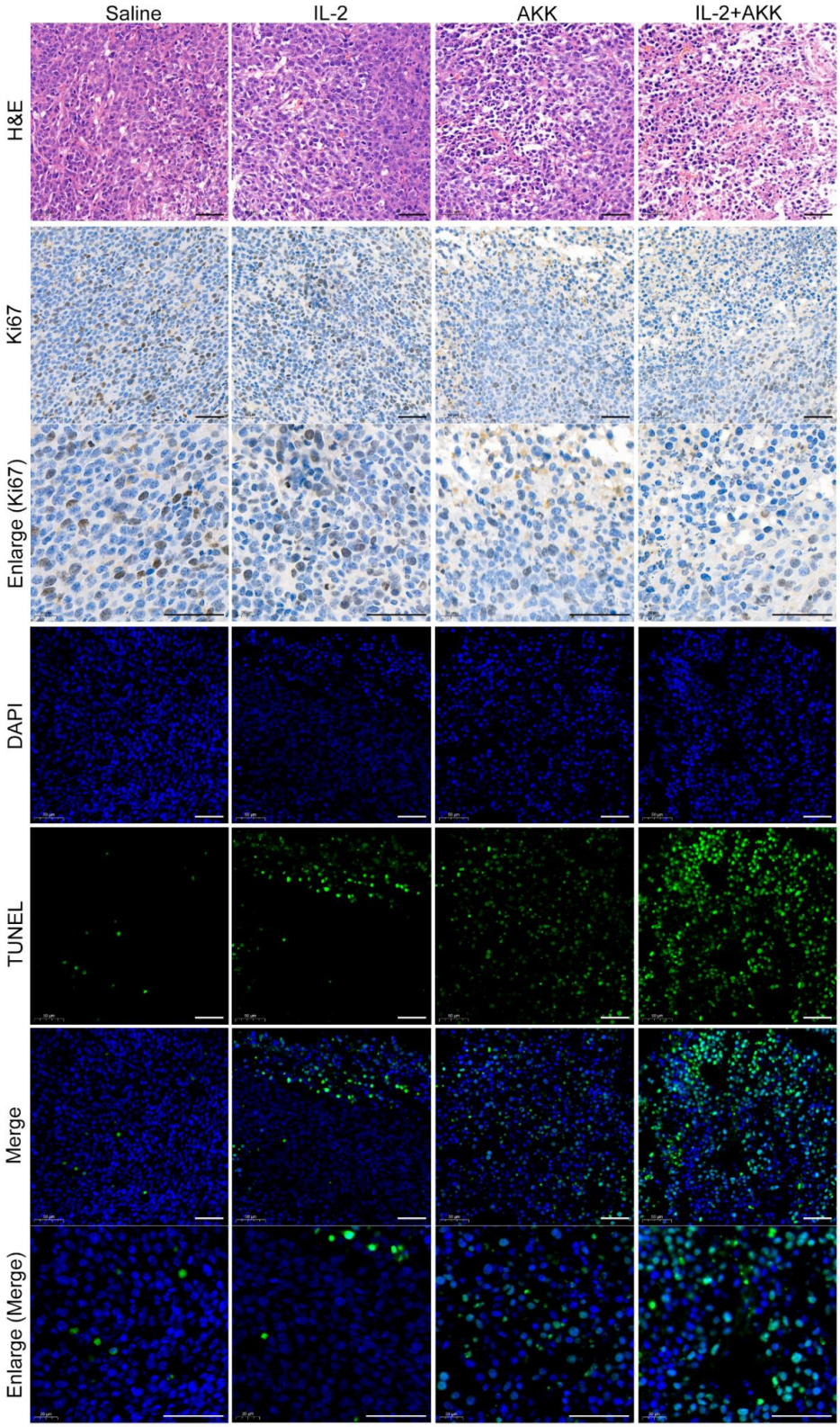

Figure S4. Representative histological staining of tumor sections from B16F10 tumor-bearing mice at the end of the experiment (200× or 400× enlargement, scale bar = 50 μm).

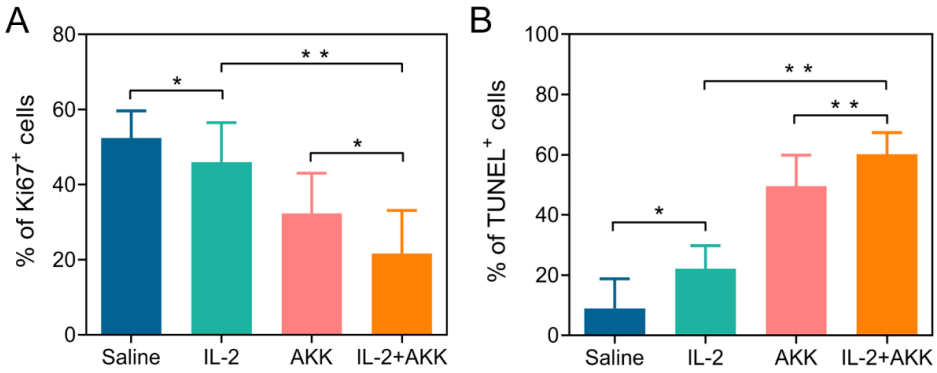

Figure S5. Quantitative analysis of Ki67⁺ cells (A) and TUNEL⁺ cells (B) in the tumor tissues collected from B16F10 tumor bearing mice among different treatment groups (n = 6). All data are shown as mean ± SD (*$P < 0.05$, ** $P < 0.01$).

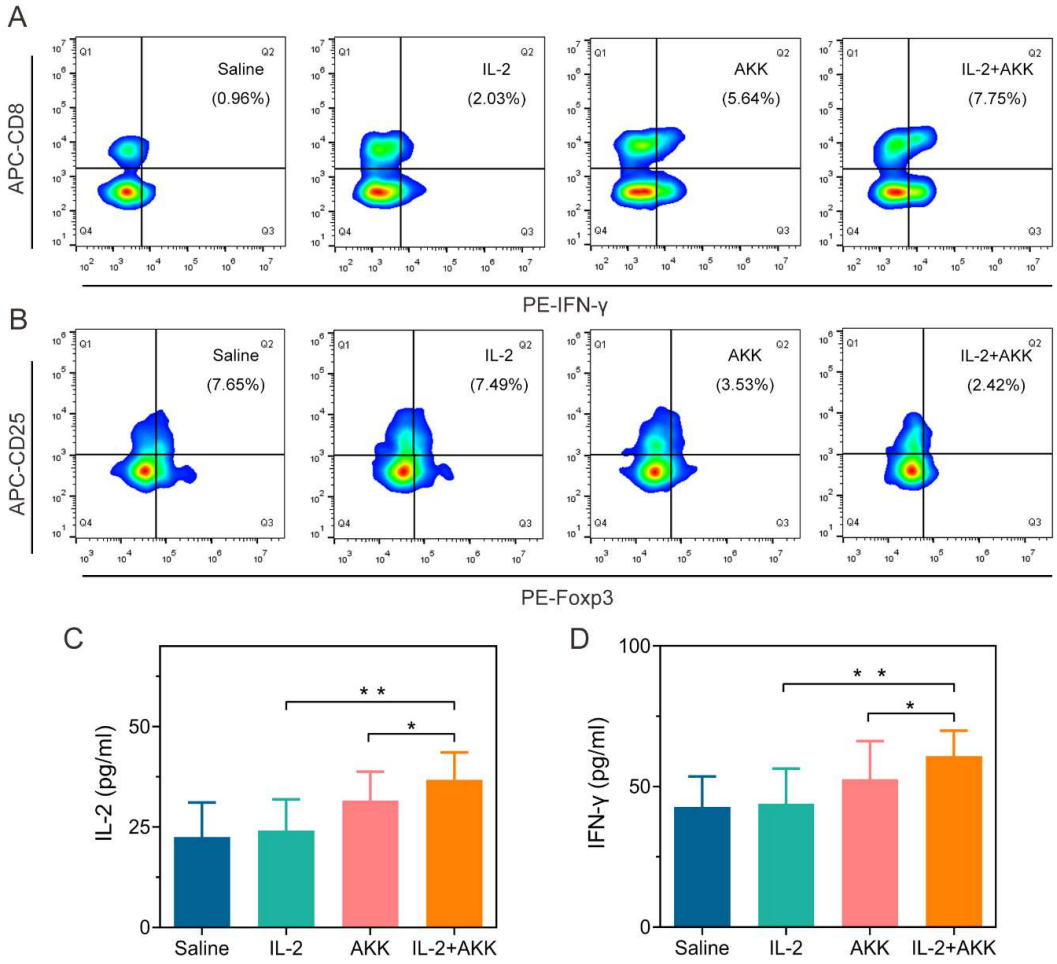

Figure S6. Alterations of tumor immune microenvironment in B16F10 tumor-bearing mice under combination therapy of IL-2 and AKK. (A) Representative flow cytometry analysis of CTLs in tumor-draining lymph nodes. (B) Representative flow cytometry analysis of Tregs in tumor-draining lymph nodes. (C, D) ELISA measurement of IL-2 (C) and IFN-γ (D) in the homogenates of tumor tissues among different groups. All data are shown as mean ± SD (n = 6, **P* < 0.05, ** *P* < 0.01).

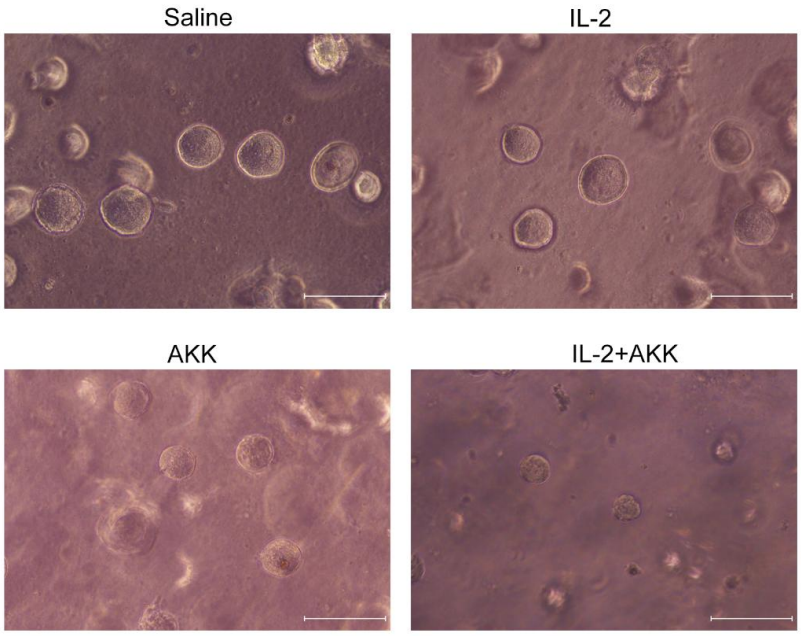

Figure S7. Representative images of tumor spheroids from CT26 tumor-bearing mice under different treatments. Tumor tissues were collected from CT26 tumor-bearing mice among different groups. Single cell suspensions were prepared from the tumor tissues, and then were seeded into soft 3D fibrin gels and incubated for 5 days. Scale bar = 50 μm.

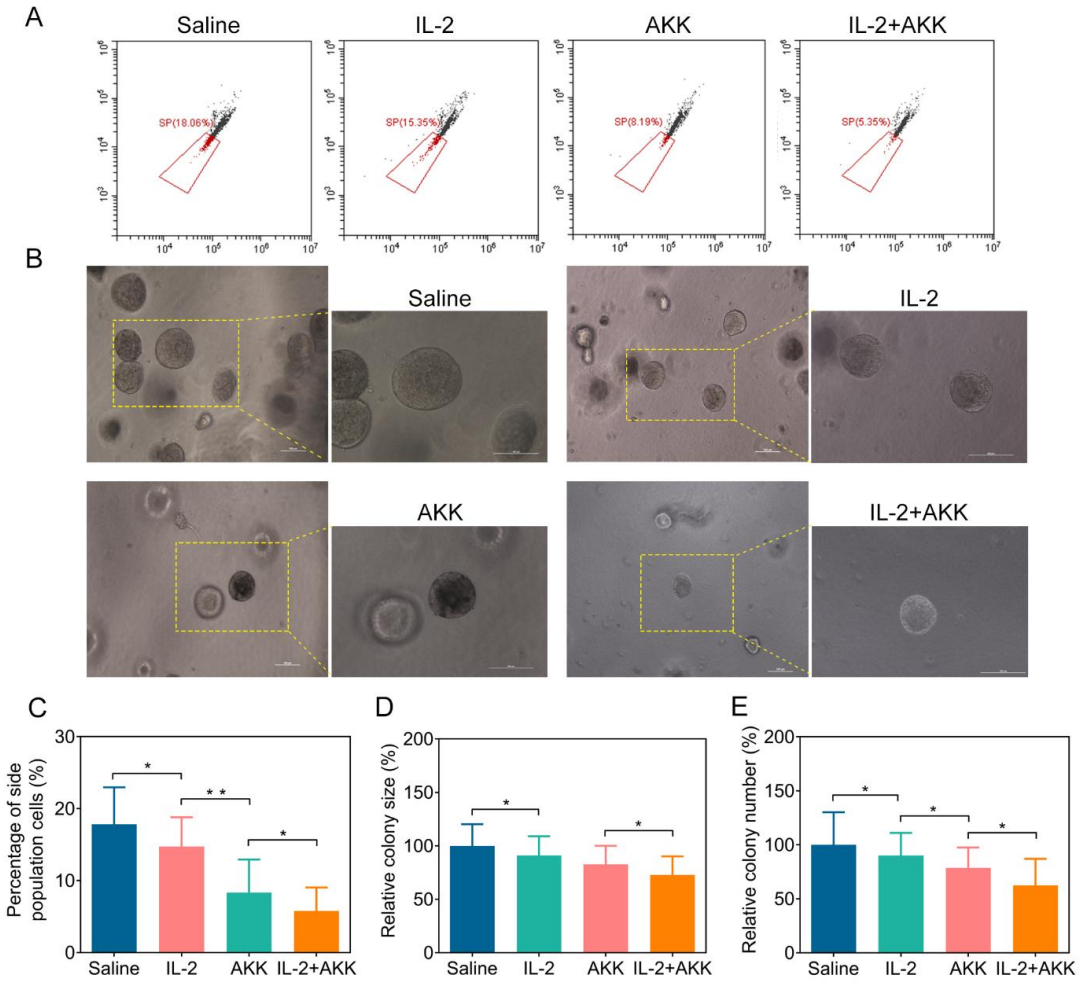

Figure S8. Side population cell analysis and tumor spheroids formation assay of tumor tissues from B16F10 tumor-bearing mice. Single cell suspensions were prepared from the tumor tissues. (A) Representative flow cytometry analysis of side population cells by flow cytometry (x-axis: PB 450-H, y-axis: Violet 660-H). (B) Representative images of spheroids of B16F10 tumor cells cultured in soft 3D fibrin gels (scale bar = 100 μm). The single cell suspensions of tumor tissues were seeded into soft 3D fibrin gels and incubated for 5 days. (C) Percentage of side population cells. (D, E) Relative colony size (D) and number (E) of tumor spheroids on the 5th day after tumor cells were seeded into the soft 3D fibrin gels. All data are shown as mean ± SD (n = 6, **P* < 0.05, ** *P* < 0.01).

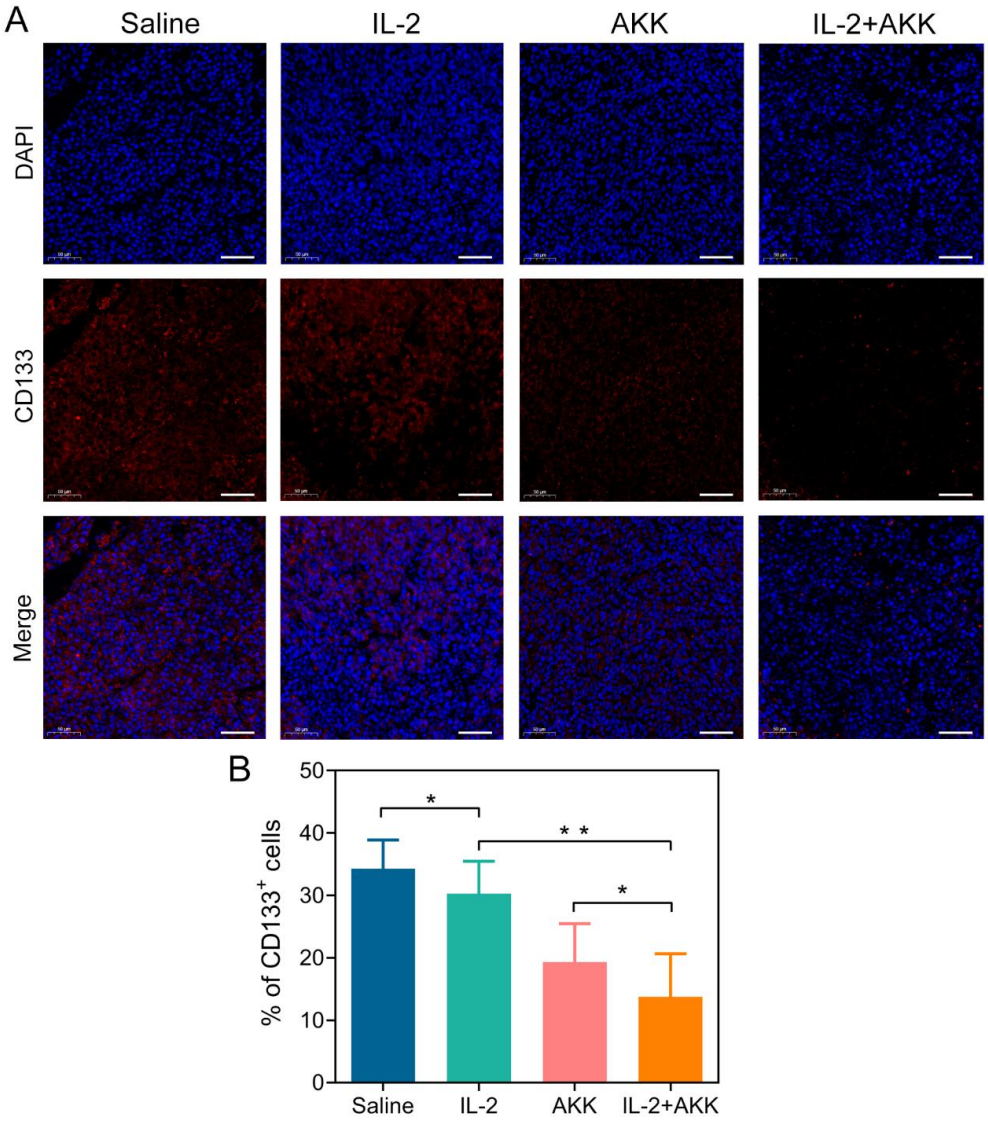

Figure S9. Representative immunofluorescent staining (A) and quantitative analysis (B) of $CD133^+$ cells in the tumor tissues collected from CT26 tumor bearing mice among different treatment groups (200×, scale bar = 50 μm). All data are shown as mean ± SD (n = 6, **P* < 0.05, ** *P* < 0.01).

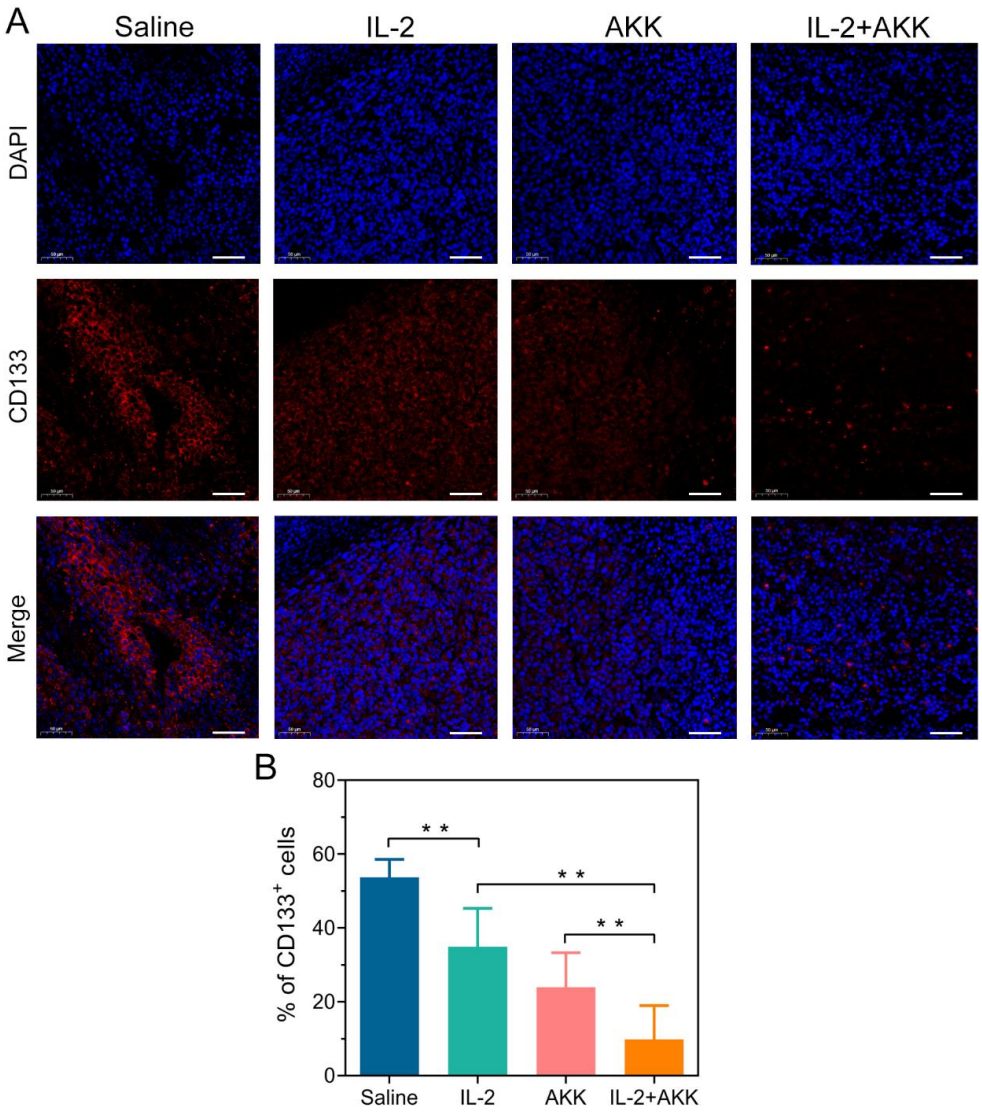

Figure S10. Representative immunofluorescent staining (A) and quantitative analysis (B) of CD133⁺ cells in the tumor tissues collected from B16F10 tumor bearing mice among different treatment groups (200×, scale bar = 50 μm). All data are shown as mean ± SD (n = 6, ** $P < 0.01$).

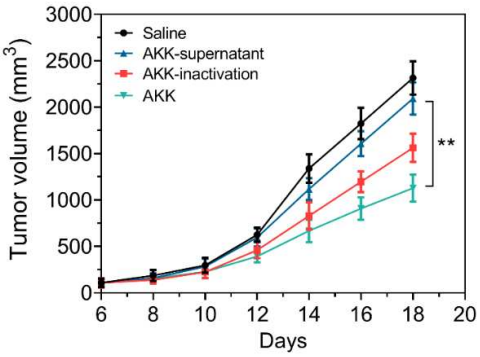

Figure S11. Tumor growth in B16F10 tumor-bearing mice treated with the pasteurized AKK and the culture supernatant of AKK (n = 6). Data are shown as mean ± SD (** $P < 0.01$).

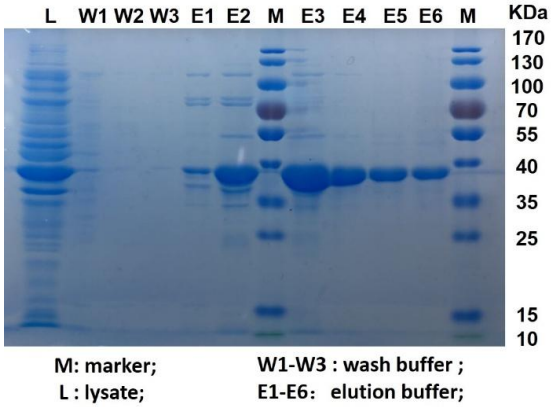

Figure S12. Purification of Amuc. The purification process of Amuc (~40 kDa) was characterized by sodium dodecyl sulfate polyacrylamide gel electrophoresis (SDS-PAGE).

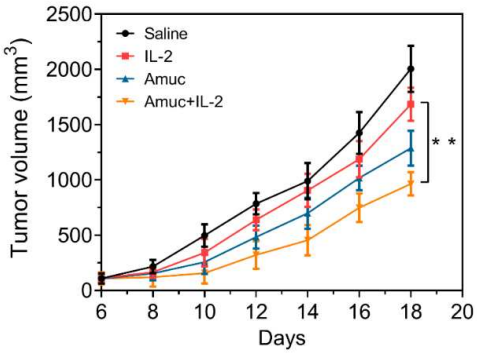

Figure S13. Tumor growth in B16F10 tumor-bearing mice treated with IL-2 and Amuc (n = 6). Data are shown as mean ± SD (** $P < 0.01$).

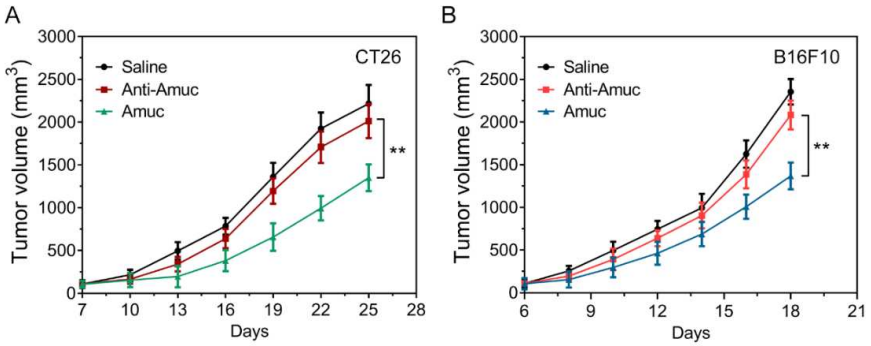

Figure S14. Tumor growth in CT26 tumor-bearing mice (A) or B16F10 tumor-bearing mice (B) treated with blocked Amuc. In the anti-Amuc group, Amuc was pretreated with anti-Amuc antibody before oral delivery to tumor-bearing mice. All data are shown as mean ± SD (n = 6, ** $P < 0.01$).

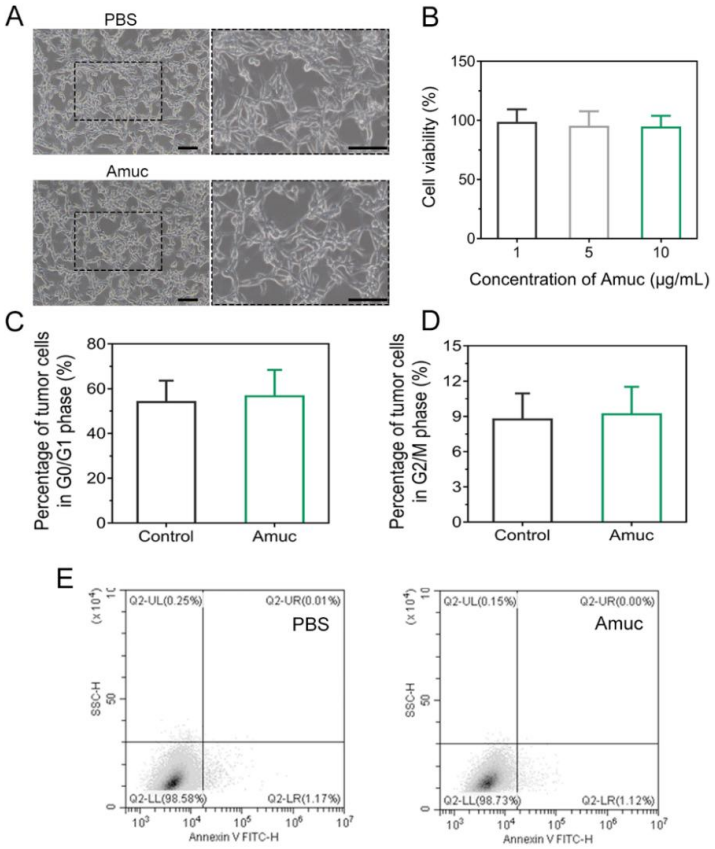

Figure S15. Effects of Amuc on CT26 tumor cells in vitro. (A) Representative images of cell morphology after Amuc treatment (100× or 200× enlargement, scale bar = 100 μm). (B) Cell viability after treatment with different concentration of Amuc for 24 hours. The viability was measured by CCK-8 method (n = 8). (C, D) Cell cycle analysis after receiving Amuc treatment for 24 hours (n = 8). (E) Representative flow cytometry analysis of apoptosis tumor cells after incubation with Amuc for 24 hours**.**

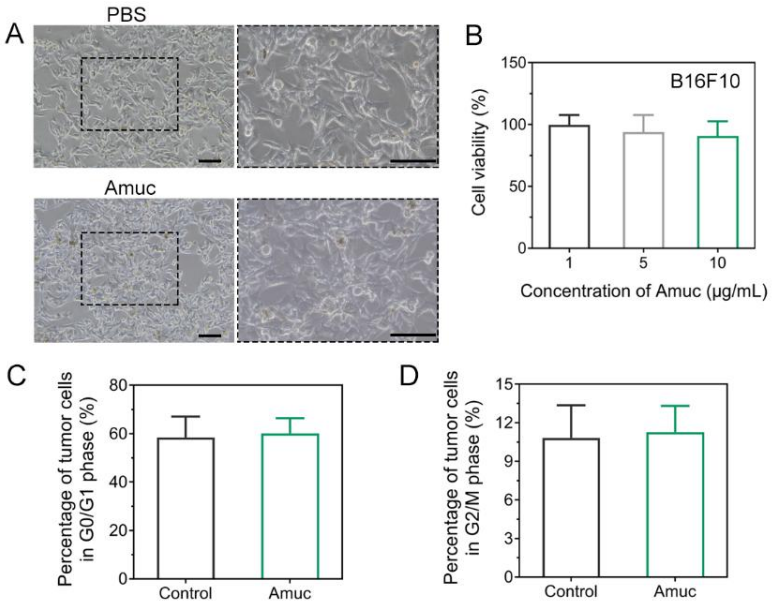

Figure S16. Effects of Amuc on B16F10 tumor cells in vitro. (A) Representative images of cell morphology after Amuc treatment (100× or 200× enlargement, scale bar = 100 μm). (B) Cell viability after treatment with different concentration of Amuc for 24 hours. The viability was measured by CCK-8 method (n = 8). (C, D) Cell cycle analysis after receiving Amuc treatment for 24 hours (n = 8).

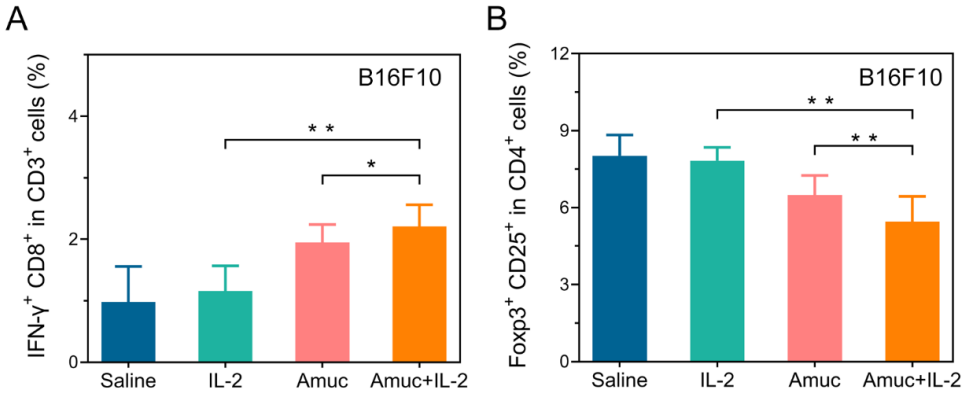

Figure S17. Alterations of tumor immune microenvironment in B16F10 tumor-bearing mice treated with IL-2 and Amuc. (A) Proportions of IFN-γ$^+$ CD8$^+$ in CD3$^+$ T cells in tumor-draining lymph nodes. (B) Proportions of Foxp3$^+$ CD25$^+$ in CD4$^+$ T cells in tumor-draining lymph nodes. Data are shown as mean ± SD (n = 6, *$P < 0.05$, ** $P < 0.01$).

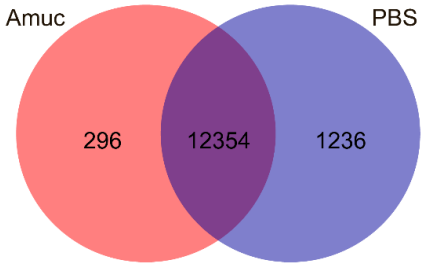

Figure S18. Venn diagram of the identified differentially expressed genes from tumor-infiltrating lymphocytes between Amuc treatment and PBS treatment.

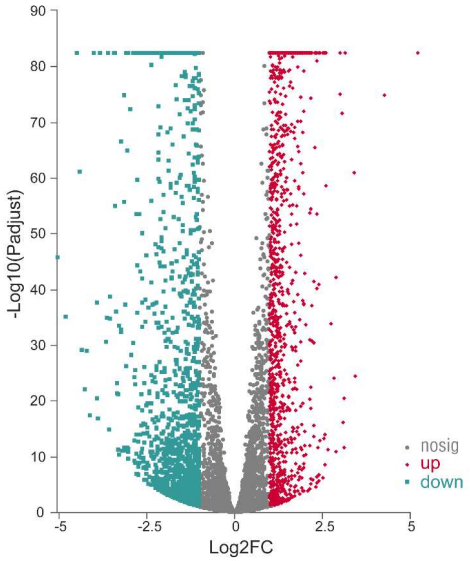

Figure S19. Volcano plots indicating the differentially expressed genes of tumor-infiltrating lymphocytes (Amuc treatment *vs* PBS treatment).

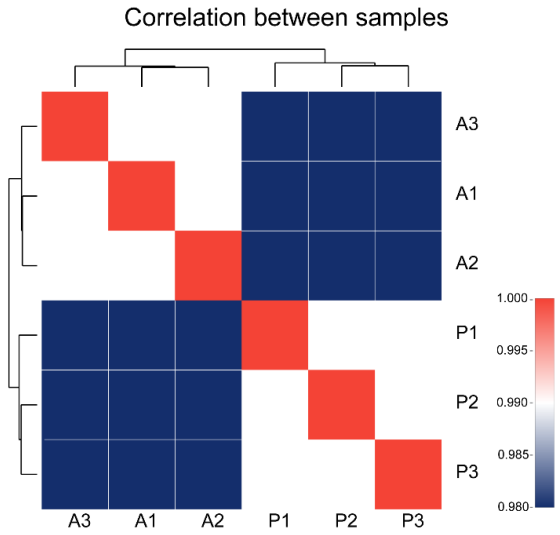

Figure S20. Correlation analysis of the transcriptomic data among different samples (A1-3: Amuc treatment; P1-3: PBS treatment).

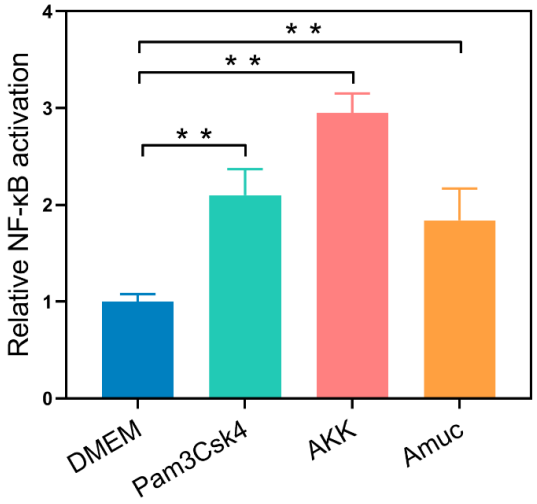

Figure S21. Stimulation effect of AKK and Amuc on TLR2-expressing HEK 293T cells in vitro. Dual-luciferase reporter gene assay for TLR2 was performed in HEK 293T cells after AKK (1×10^7 CFU/mL) or Amuc (10 μg/mL) treatment. Data are shown as mean ± SD (n = 6, **P* < 0.05, ** *P* < 0.01).

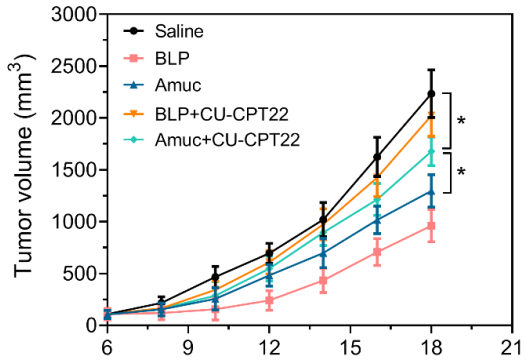

Figure S22. Tumor growth in B16F10 tumor-bearing mice under different treatments (n = 6). The synthetic bacterial lipoprotein (BLP, a TLR1/TLR2 agonist) was used as the positive control and CU-CPT22 (a TLR1/TLR2 antagonist) as the negative control. Data are shown as mean ± SD (*P < 0.05).

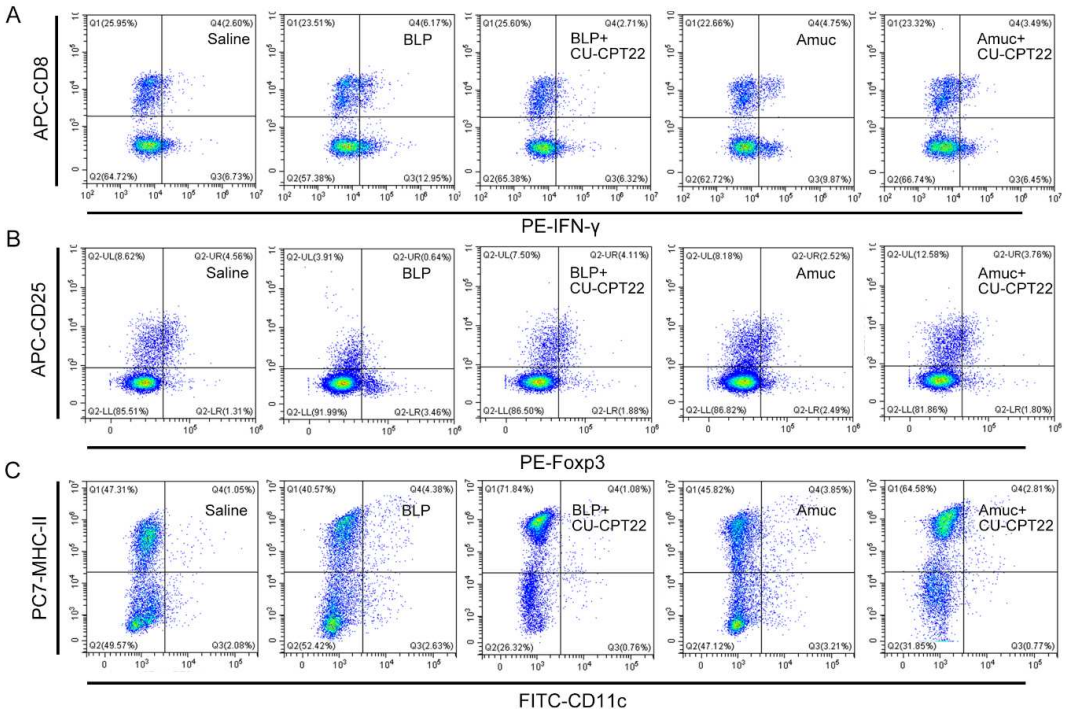

Figure S23. The role of TLR2 pathway in Amuc induced alterations of the tumor immune microenvironment. (A) Representative flow cytometry analysis of cytotoxic effector T cells in tumor-draining lymph nodes (Gated on CD3). (B) Representative flow cytometry analysis of Treg cells in tumor-draining lymph nodes (Gated on CD4). (C) Representative flow cytometry analysis of activated DCs in tumor-draining lymph nodes. Data are representative of the results in both CT26 and B16F10 tumor-bearing mice.

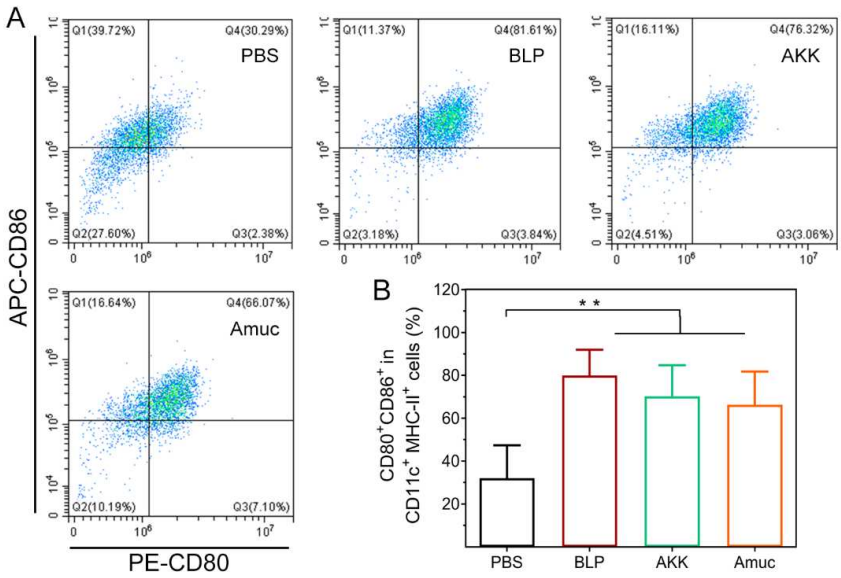

Figure S24. The role of TLR2 pathway in Amuc-induced activation of BMDCs in vitro. BMDCs were incubated with PBS, BLP (5 μg/mL, a TLR1/TLR2 agonist), AKK (1×10^7 CFU/mL) and Amuc (10 μg/mL) for 48 h prior to flow cytometry analysis (n = 6-8). (A) Representative flow cytometry analysis of the activated DCs. (B) Proportions of $CD80^+$ $CD86^+$ in $CD11c^+$ $MHC\text{-}II^+$ cells in BMDCs. Data are shown as mean ± SD (** $P < 0.01$).

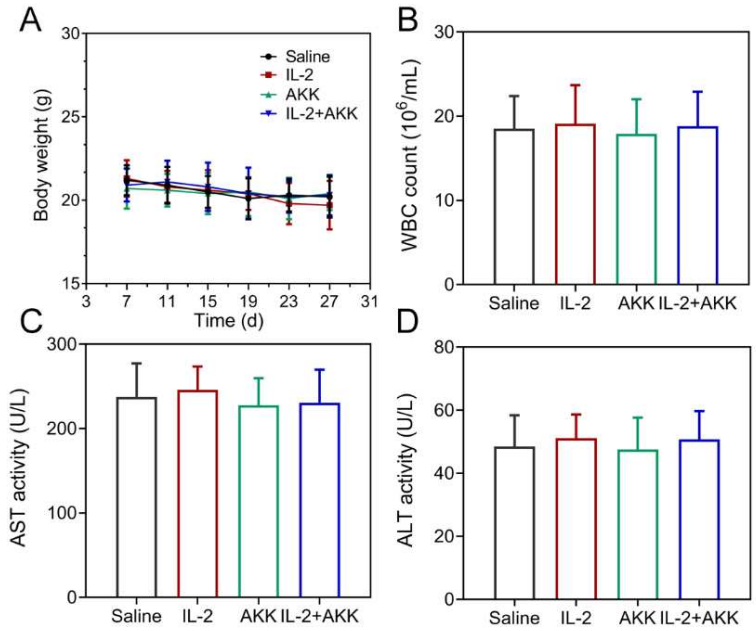

Figure S25. Body weight and blood biochemical analysis in CT26 and B16F10 tumor-bearing mice receiving different treatments (n = 6). Data are representative of the results in both CT26 and B16F10 tumor-bearing mice.

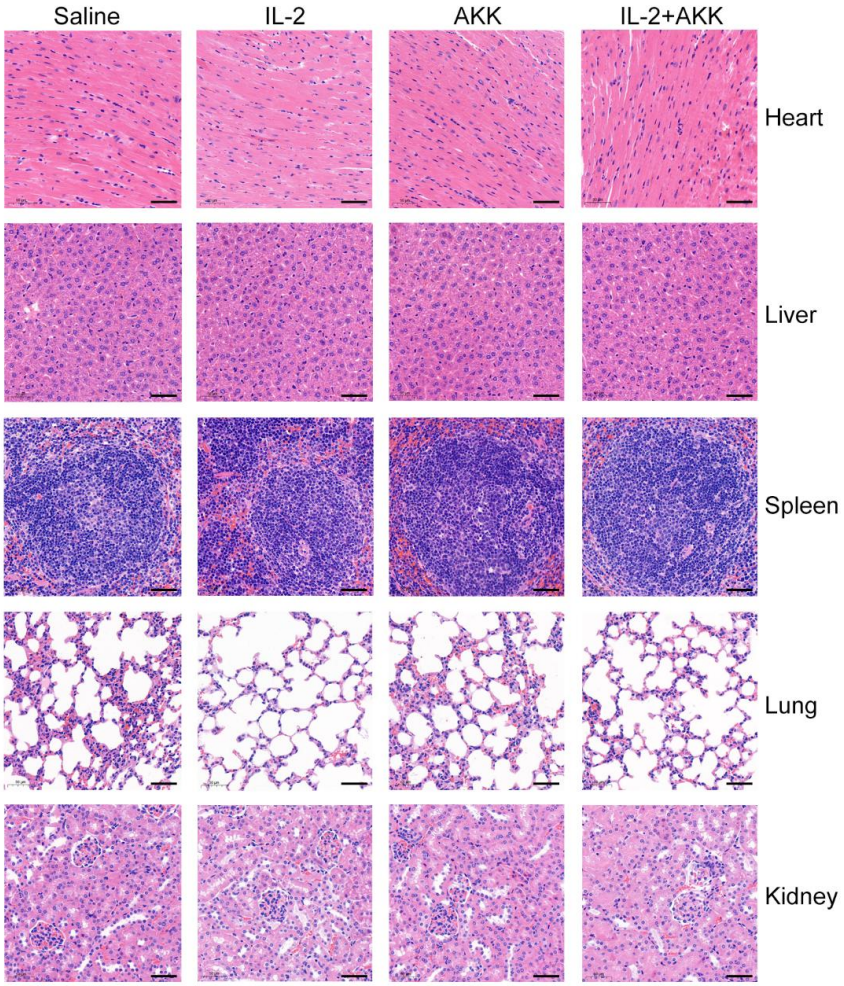

Figure S26. Representative images of H&E staining of tissues from main organs (heart, liver, spleen, lung, and kidney) in CT26 tumor-bearing mice after treatment with IL-2 and AKK (n = 4-6, 200×, scale bar = 50 μm).

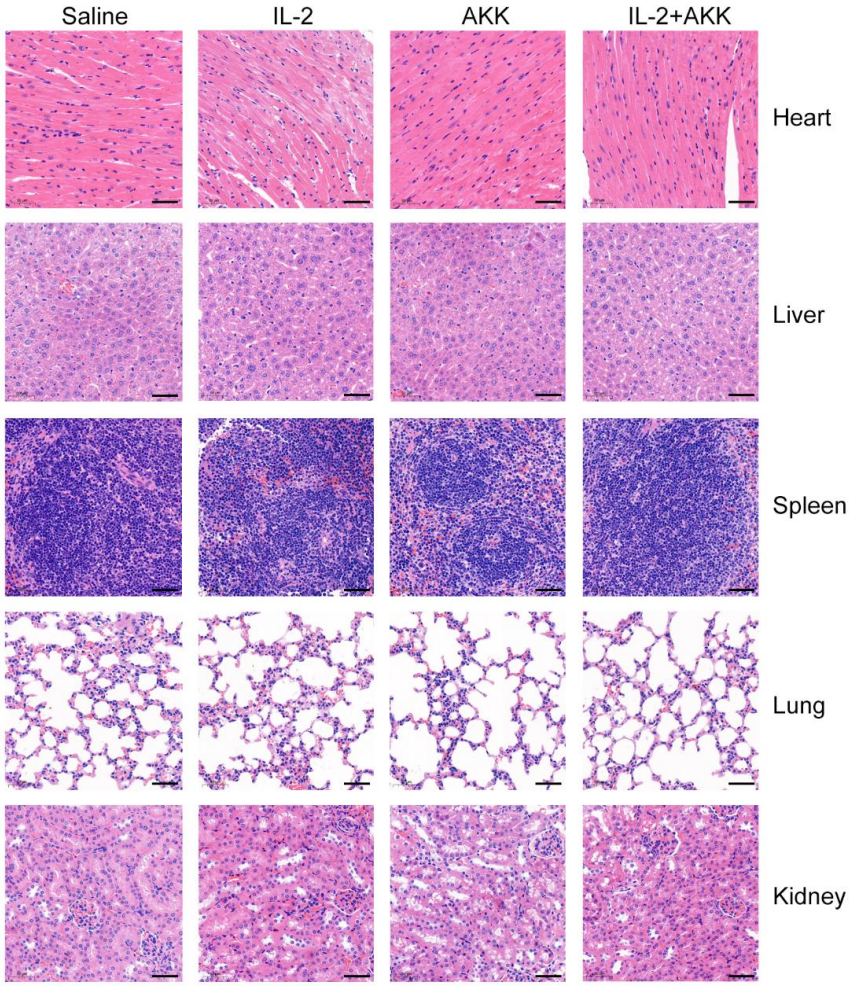

Figure S27. Representative images of H&E staining of tissues from main organs (heart, liver, spleen, lung, and kidney) in B16F10 tumor-bearing mice after treatment with IL-2 and AKK (n = 4-6, 200×, scale bar = 50 μm).

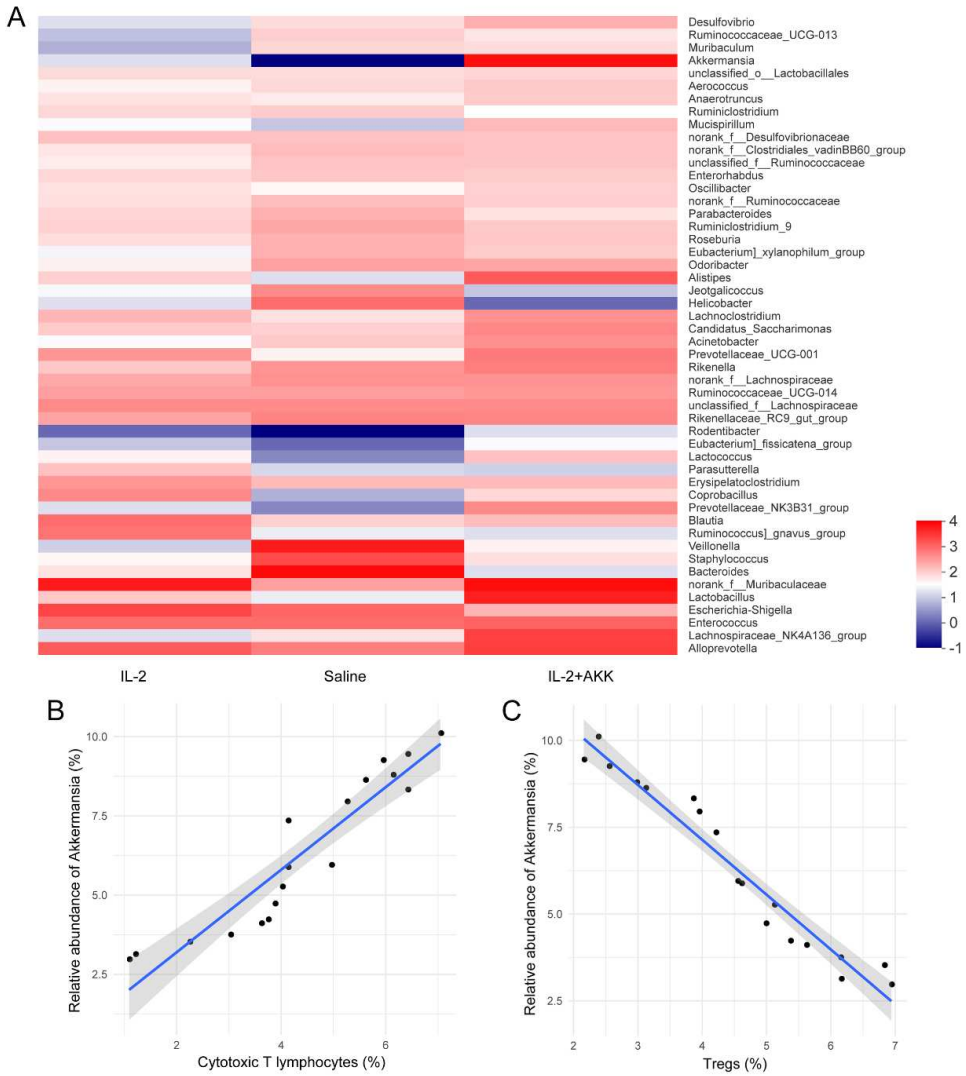

Figure S28. Effects of AKK pretreatment on regulating gut microbiota homeostasis in the context of IL-2 treatment. (A). Community heatmap analysis at the genus level among different treatment groups (n = 6). Color gradient is used to show the variation of bacterial annotation and abundance information among different treatment groups. Correlation analysis between the relative abundance of AKK and the percentage of (B) cytotoxic T cells ($r = 0.9379$, $p < 0.05$) and (C) Tregs ($r = -0.9732$, $p < 0.05$) in tumor-draining lymph nodes among different treatment groups.

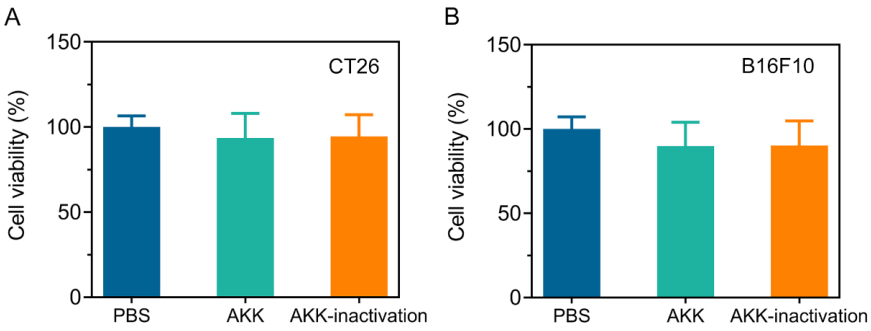

Figure S29. Effects of AKK and pasteurized AKK on CT26 (A) and B16F10 (B) tumor cells in vitro. After treatment with alive AKK (1×10^7 CFU/mL) and pasteurized AKK (an equivalent dose of alive AKK was inactivated by pasteurization at 70 °C for 30 min) for 24 hours. Cell viability was measured by CCK-8 method (n = 8).

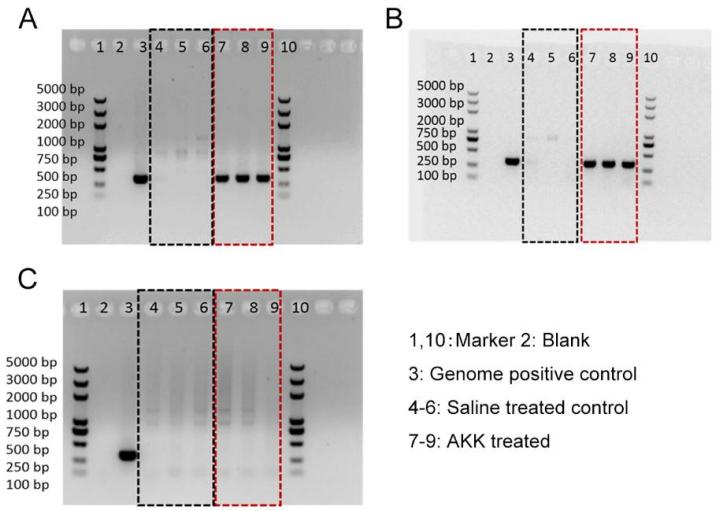

Figure S30. AKK detection in CT26 tumor-bearing mice. DNA was extracted from intestinal content (A), fecal samples (B) and tumor tissues (C), and amplified with AKK specific primers (~320 bp) between tumor-bearing controls and AKK treated group (n = 3).

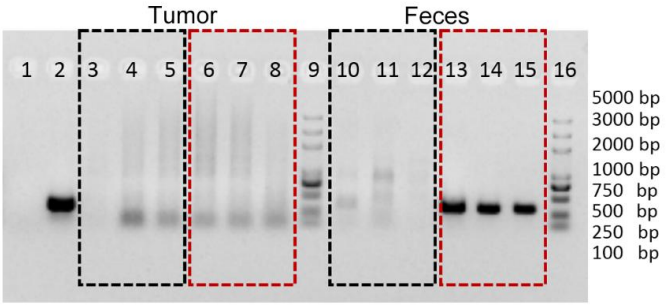

1: Blank 2: Genome positive control 9,16: Marker

3-5: Saline treated control 6-8: AKK treated group

10-12: Saline treated control 13-15: AKK treated group

Figure S31. AKK detection in B16F10 tumor-bearing mice. DNA was extracted from tumor tissues and fecal samples and amplified with AKK specific primers (~320 bp) between tumor-bearing controls and AKK treated group (n = 3).

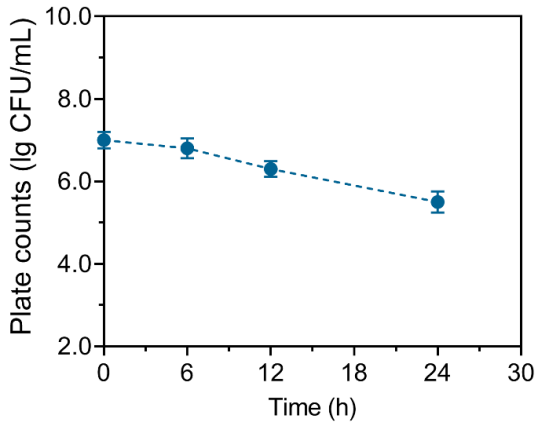

Figure S32. Survival of AKK after exposure to oxygen over time. AKK co-cultured with tumor cells were exposed to ambient air and incubated at 37 °C, which was the same condition as the experiments on CRC patients derived ex-vivo tumor tissues. At predetermined time points over a period of 24 h, the co-culture suspensions were collected and serially diluted 10-fold with PBS. 10 μL aliquots of each dilution were spotted on mucin-based plates. Survival rate of AKK was determined by CFU counts on the plates.

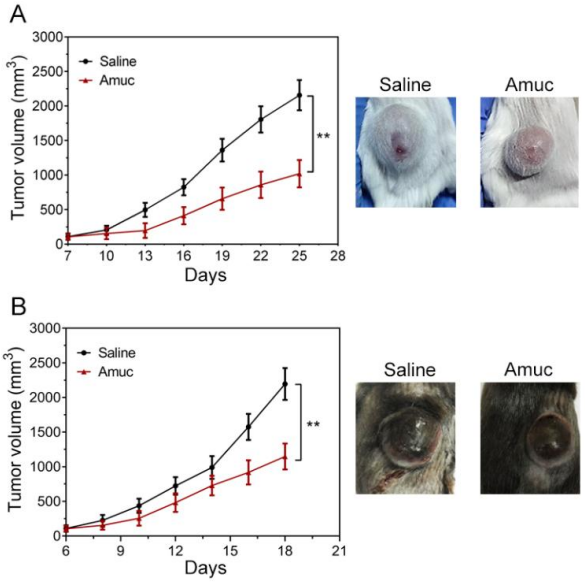

Figure S33. Tumor growth in CT26 (A) or B16F10 (B) tumor-bearing mice treated with in situ injection of Amuc. Data are shown as mean ± SD (n = 6, ** $P < 0.01$).

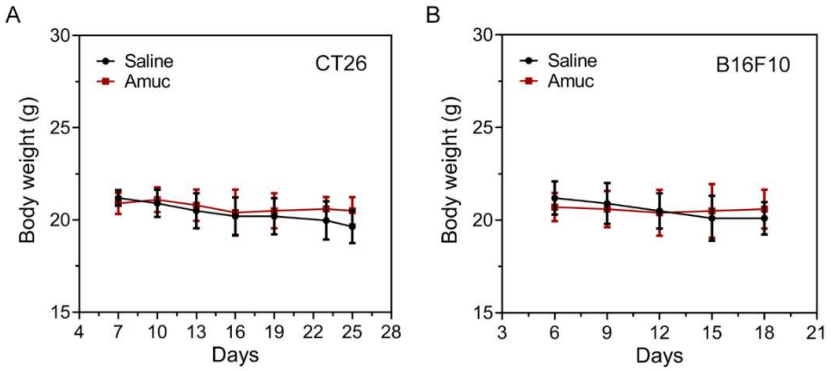

Figure S34. Body weight change of CT26 (A) or B16F10 (B) tumor-bearing mice after in situ injection of Amuc. Data are shown as mean ± SD (n = 6).

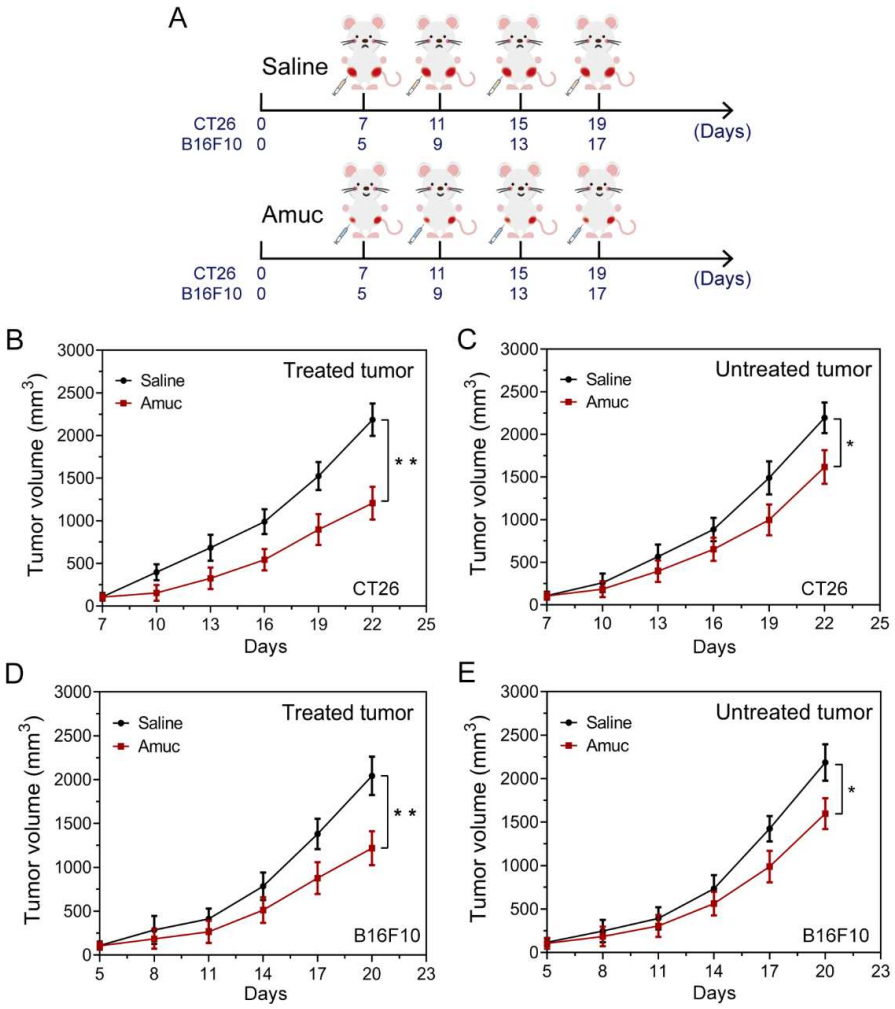

Figure S35. In situ injection of Amuc induces systemic antitumor immune responses in CT26 and B16F10 tumor bearing mice (n = 6). Amuc was injected into one side of the tumors in bilateral tumor models. Saline was injected into the same side in the control group. Tumors on the other side remain untreated in both groups. (A) Experimental scheme of single-flank in situ injection in tumor-bearing mice. (B, C) Tumor growth on the treated side (B) and untreated side (C) in CT26 tumor-bearing mice. (D, E) Tumor growth on the treated side (D) and untreated side (E) in B16F10 tumor-bearing mice. Data are shown as mean ± SD (*$P < 0.05$, ** $P < 0.01$).

Supplementary table 1

Table S1. Clinical Characteristics of the CRC patients.

CRC cases			
Age	66	55	51
Sex	Male	Male	Female
Body mass index	20.6	26.2	25.9
CRC stage	2	3	3
TNM stage	T4N0M0	T4N2M0	T4N2M0
Site of tumor	Sigmoid	Sigmoid	Ascending